Evolution of normal fault systems in physical analogue experiments

Renate Eimind Tveit

Thesis for the degree

Master of Science

Department of Earth Science

University of Bergen

March, 2019

Abstract

Analogue plaster modelling is used to study the normal fault growth in the extensional regime in this MSc thesis. Using Plaster of Paris, which is well suited to produce small-scale structures illustrating the complexity of the evolution of faults in the extensional regime.

The growth in length and maximum displacement is documented and tracked for several fault segments throughout the experiment and plotted in to a diagram showing the ratio between length and maximum displacement.

Four stages are characterized by studying the displacement-length trajectories in detail. The first stage is defined by fault growth by lengthening with minimal displacement accumulation. Stage two constitute a period of displacement accrual and limited lengthening. The third stage is a renewed period with lengthening and a low-rate displacement accumulation. The last stage is defined by linkage and for these experimental models assembly of the main fault.

The displacement-length trajectories are compared with the two well-known growth of normal fault models, the 'propagating' and the 'constant-length' fault growth models. The propagating fault growth model suggest that faults grows by increasing synchronously in length and displacement ratio. The constant length model propose that faults grows their near-final length early in the deformation history and then enters a period with displacement accrual.

An overall trend in the displacement-length diagram suggest that there are two main periods in the evolution in the fault growth. The first period is defined by the propagational fault growth model and the second period contains the constant-length fault growth model
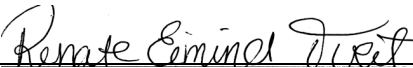
Acknowledgement

Bergen 18.03.2019

Renate Eimind Tveit

Contents

CHAPTER 1 – INTRODUCTION

1.1 Introduction

In this thesis, analogue modelling of the extensional regime is used in this project to investigate the geometry and growth of normal faults.

Normal fault growth is studied by investigating the tip-propagation and segment linkage between fault segments and subsegments. This also includes quantify the fault length and heave. There are mainly two growth models that are preferred, the 'propagating' and 'constant-length' fault models (Fig. 2.3)(Rotevatn et al., 2018). The former fault growth model describes that the fault increases synchronously between length and displacement, while the latter propose that the fault establishes its almost full length early, thus enters a phase of displacement accruing.

By using analogue models to study normal faults, is it possible to follow the whole evolution of the fault, from it nucleates through the surface and until it is fully developed. Every step of the experiment is documented by images, so it is possible to store information of the entire formation process to the fault. The material used in this experiment is made of plaster and barite. The plaster consists of fine-grained material which solidifies as the experiment continues. This provides the opportunity to study small-scale structures based on the experiment and also preserve information in the end result of the model

The understanding of how faults grow is limited to observation of outcrops in nature and seismic interpretation. In nature are the information restricted to outcrops mainly in 2-dimention, while seismic interpretation of fault can be observed both in 2- and 3-dimention but is limited by resolution. Both of these research methods show the end result of a geological event and not the evolution of the event. Restoration and balancing are often used to form a hypothesis for how they have occurred, but none of these options provides an accurate description of the occurrence of the events, and analogue modelling is therefore helpful to gain insight to the evolution of the faults.

The analogue experiments used for this project were performed in 2015 for a sister project also focusing on the extensional regime, and the results of this modelling is analysed in this thesis. The implementation took place at the Department of Earth Science at the University of Bergen.

1.2 Aims and objectives

The aim of this project is to study how normal faults grow to and to study their evolution in displacement-length (D-L) space. The main objectives are listed below:

i)   Examine how the faults grow in the plaster model by studying the lengthening, displacement accruing and the linkage for several faults in detail

ii)   Quantify the measurements extracted from the experiment, mainly the length and heave of the fault segments

iii)   Compare the fault growth result to existing models for fault growth

iv)   Compare the linkage and relay ramp breach

v)   v) investigate the D-L growth behaviour of faults

vi)   vi) Use the result from the model to compare with global D-L dataset

CHAPTER 2 - EXTENSIONAL FAULTING

2.1 Introduction

The aim of this chapter is to provide theory about the extensional faulting, focusing on the normal fault structures, their geometry and growth pattern.

2.2 Extensional regime

An extensional regime is an area that is stretched in the horizontal direction. This is often related to tectonic processes, but may also be caused by gravitational sliding. Normal faults are the main structure formed in this regime and forms in the brittle part of the crust (Fossen, 2010).

2.2.1 Architecture of a normal fault

A normal fault forms when the hanging wall is lowered relative to the footwall. The offset between the hanging wall and footwall in horizontal direction is called heave and in the vertical direction is called throw (Fig. 2.1). The surface onto which offset is localised is the fault surface, which sits between the hanging wall and footwall (Fossen, 2016). A fault zone can be divided into regions based on its sum of properties of individual small-scale tectonic structure or combinations of structures (Braathen, et al., 2009).
The fault core is a high-strain zone and is where most of the displacement are accommodated (Caine, Evans, & Forster, 1996). This zone can vary from smaller than a millimetre to several meters in thickness (Fossen, 2010)). The core contains elements of deformation band, slip surface, fracture, cleavage, stylolite, smear along fault etc (Braathen, et al., 2009). Damage zone surrounds the core and contains the brittle deformation structure as deformation band, fracture, stylolite etc. (Braathen, et al., 2009). Occasionally deflected layers surround the damage zone, called a drag zone. It consists of the ductile deformation of strain zone

associated with the structure (Fossen, 2010)) and a protolith zone is the original rock without any deformation.
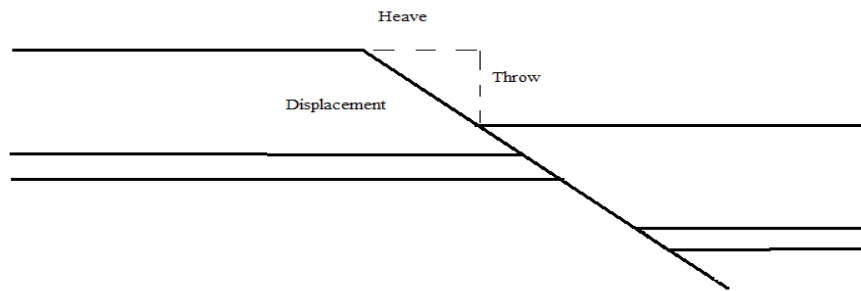
Figure 2.1: Idealized normal fault architecture.

The key dimensional parameters of a normal fault are represented by maximum displacement and length (J. Walsh et al., 2003). There is a positive correlation between displacement and length (Cowie & Scholz, 1992a). An elliptical fault plane can be used to illustrate the ideal normal fault (Fig. 2.2a). The elliptical circles represent fault-tip and distribution of displacement. The maximum displacement would be zero at the fault tip and usually increases towards the center of the fault (Fig. 2.2a), but the displacement varies within the fault surface (Barnett et al., 1987).

Kim and Sanderson (2005) proposed a unified terminology for fault description that can be used regardless of their kinematics (Fig. 2.2a). The longest horizontal dimension in the ellipse is called fault length (L) and the plane that is exposed in the surface is characterized as the fault trace length (L'). The longest vertical dimension in the ellipse for the fault plane is measured as the fault height (H) and fault trace height (H') is represent the exposed length in in cross-section.
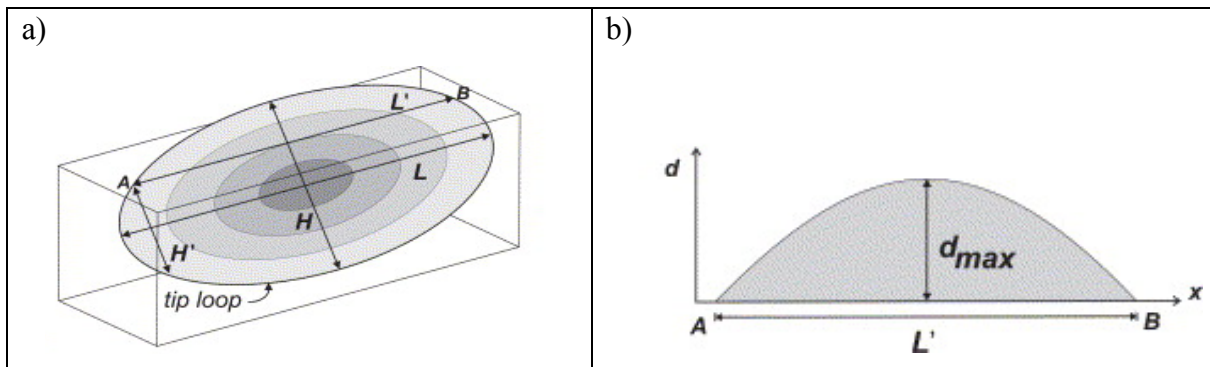
Figure 2.2: a) shows an elliptical fault surface that illustrates the distribution of displacement within the fault plane. Also presenting where the maximum length (L) and height (H) along with the trace length (L') and trace height (H') are measured. b) Shows a displacement (D) – length (L) plot. From (Kim & Sanderson, 2005)

Several factors are proposed to control the ratio of maximum displacement (Dmax) and fault length (L) (Kim & Sanderson, 2005). Different types of material properties can become effective barriers on propagation of small- scale faults. Scaling of fault in a sedimentary rock can be affected by its lithology (Steen and Andersen, 1999) (Wilkins & Gross, 2002). Normal and thrust faults has slightly smaller ratio than a strike-slip fault, when the position and direction of measurements are included (Kim & Sanderson, 2005). Fault propagation may alter the ratio between displacement and length, because the mechanical interaction and localization of strain on larger faults (e.g., Cowie and Scholz, 1992b; Willemse et at., 1996; Walsh et at., 2002, 2003b) in turn means that it depends on segmentation and linkage (Sibson, 1989; Cowie and Scholz, 1992b) fault scale (Clark and Cox, 1996; Kim et al., 2000) and reactivation of faults.

2.2.2 Normal fault growth

Normal faults start to grow from small weaknesses as fracture, joints, dikes, etc, in the rock.
Forces affects these small structures and activates them to propagate and interact with nearby
small structures and fault segments, creating larger fault segments.
Two main fault growth models are presented on how the normal faults grows, the
'propagating' and 'constant-length' fault model (Fig. 2.3) (Rotevatn et al., 2018).
The propagating fault model (Fig. 2.3A) (also known as the isolated fault model) propose that
the fault grows by increasing synchronously in length and displacement (Fig. 2.3c and 2.4)
(Jackson et al., 2017; Rotevatn et al., 2018; J. Walsh et al., 2003; J. Walsh et al., 2002). These
faults propagate geometrical and kinematically isolated from each other and links by
overlapping and interacting (Giba et al., 2012).
The constant-length fault model (B) (also known as the coherent fault model) establishes its
near-final length early in its slip history and then moves in to a phase where the fault mainly
accumulate a displacement (Fig. 2.3d and 2.4) (Jackson et al., 2017; Rotevatn et al., 2018; J.
Walsh et al., 2003; J. Walsh et al., 2002). These fault segments depend on the surrounding
fault segments and propagate kinematically and geometrical related to each other (Giba et al.,
2012).

The fault growth models are shown in figure 2.3 and presents the breaching in the surface by
normal fault growth by three timesteps (T1-T3). The fault growth illustrates how normal fault
propagate in the surface in map-view (i), strike -projection (ii) and in a displacement-ratio
plot (iii). It is divided in to three timesteps (T1-T3). At the final timestep (T3) have the faults
in both of the models the same length, displacement and shape. This makes it difficult to
distinguish which of the illustrated models has occurred at T3.

Also, both 'propagating' and 'constant-length' fault model can be schematic compared in the
same diagram by using the displacement (heave for this project) and length diagram (Fig.
2.4). Fault growth that fall in between these two fault growth models are called hybrids and
consists of both the fault growth terms (Rotevatn et al., 2018). The gradient of the relationship
between length and heave for hybrid growth is partitioned between sub-horizontal and sub-
vertical fault growth (Fig 2.4). By using a log-log plot of the relationship between the length

and displacement it is possible to compare fault growth in analogue modelling with faults that occur in the nature (Fig. 2.5).
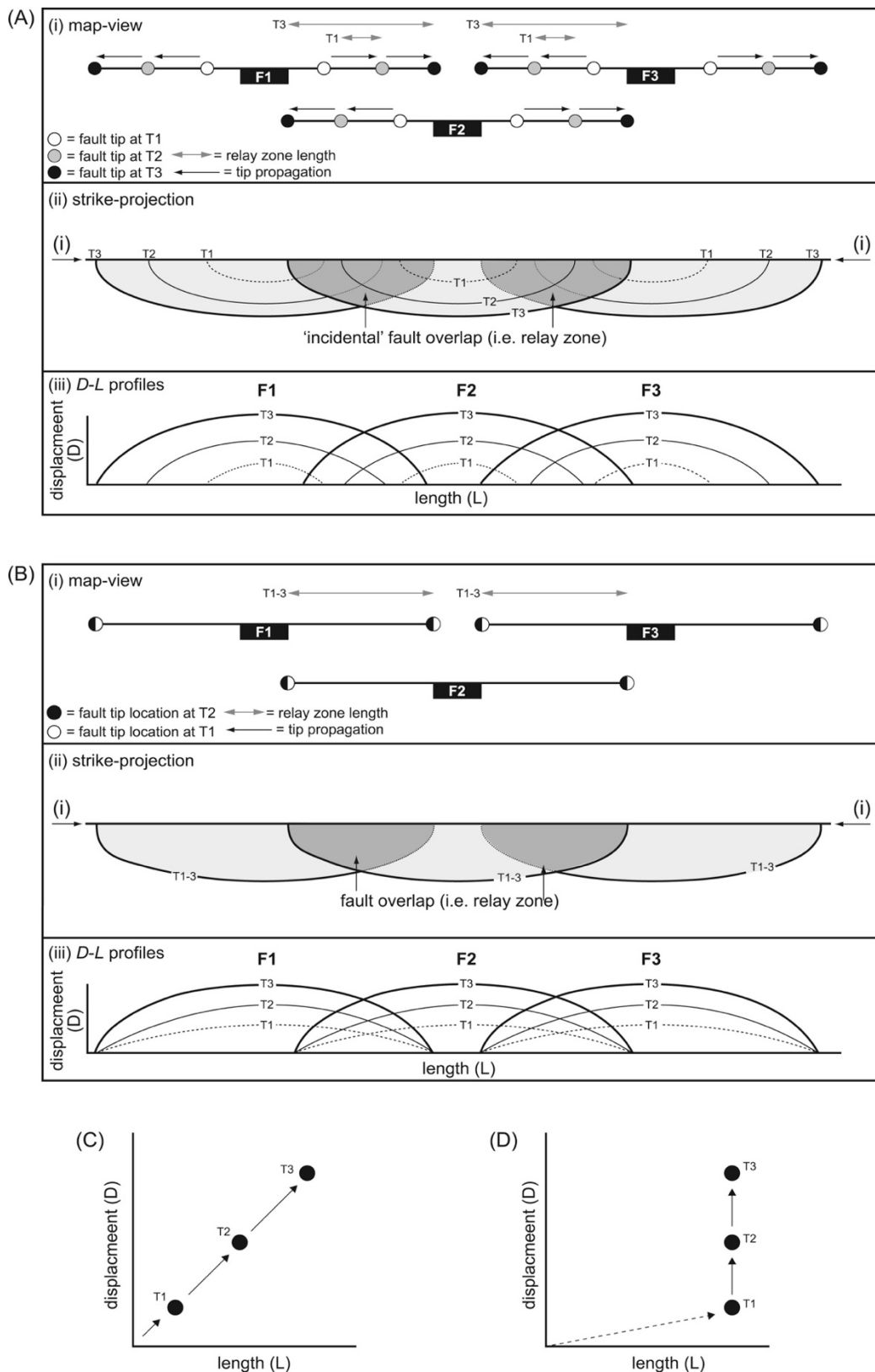
Figure 2.3: Models illustrating the 'propagating' (A) and the 'constant-length' (B) normal fault growth. The geometrical and evolutionary aspects is presented in a map-view(i), strike-projection (ii) and in a D-L profiles(iii). Three faults (F1, F2 and F3) are described with three timesteps (T1, T2 and T3). At the end is the D-L plot for each of the model. From (Rotevatn et al., 2018)
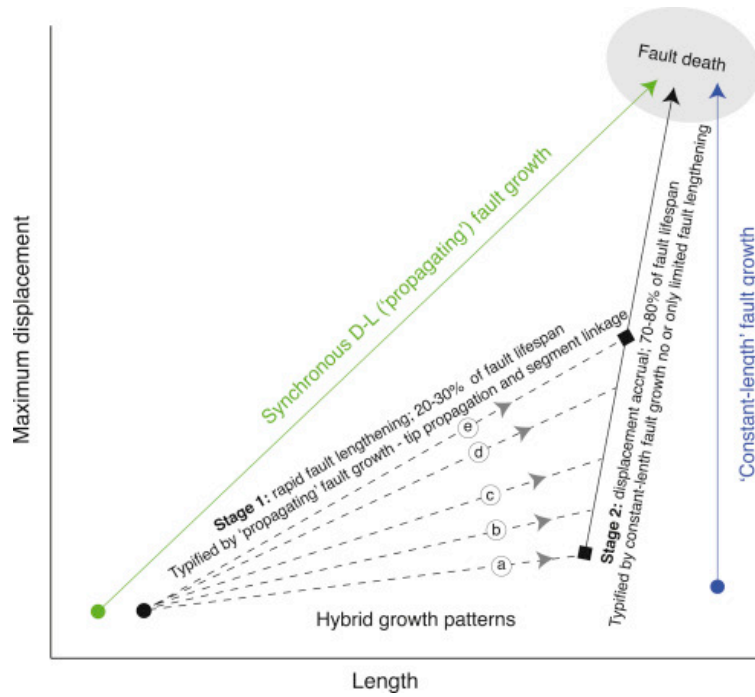
Figure 2.4: Schematic illustration of a normal fault growth including the propagating trajectory and the constant-length trajectory. From (Rotevatn et al., 2018)
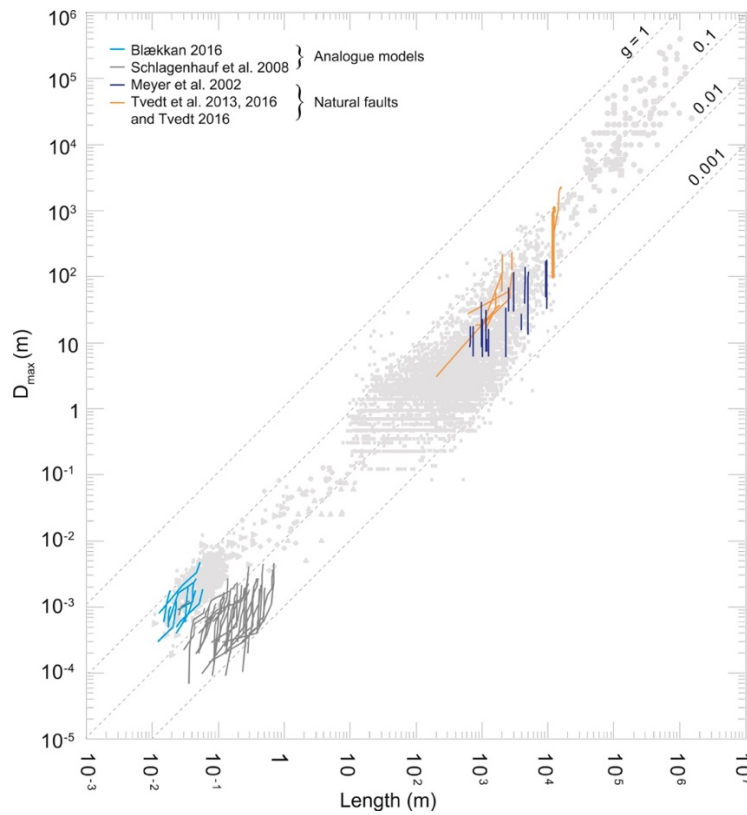
Figure 2.5: is a global D-L dataset plotted by Rotevatn et al. (2018) for both analogue models and faults in the nature.

Linkage between fault segments occur through geometric linkage in the segmented surface or by kinematic linkage in approaching segments tips or relay ramps. Soft-linkage is presented as overlapping fault that intersect in the sub-surface achieved by strain distributed in the host rock (Fig. 2.6a-b, stage 2) (J. J. Walsh & Watterson, 1991). The linkage cannot be observed in the surface. Hard-linkage is characterized as physical intersection between two or more faults segments and is visible in the surface (Fig. 2.6a-b, stage 3) (J. J. Walsh & Watterson, 1991).
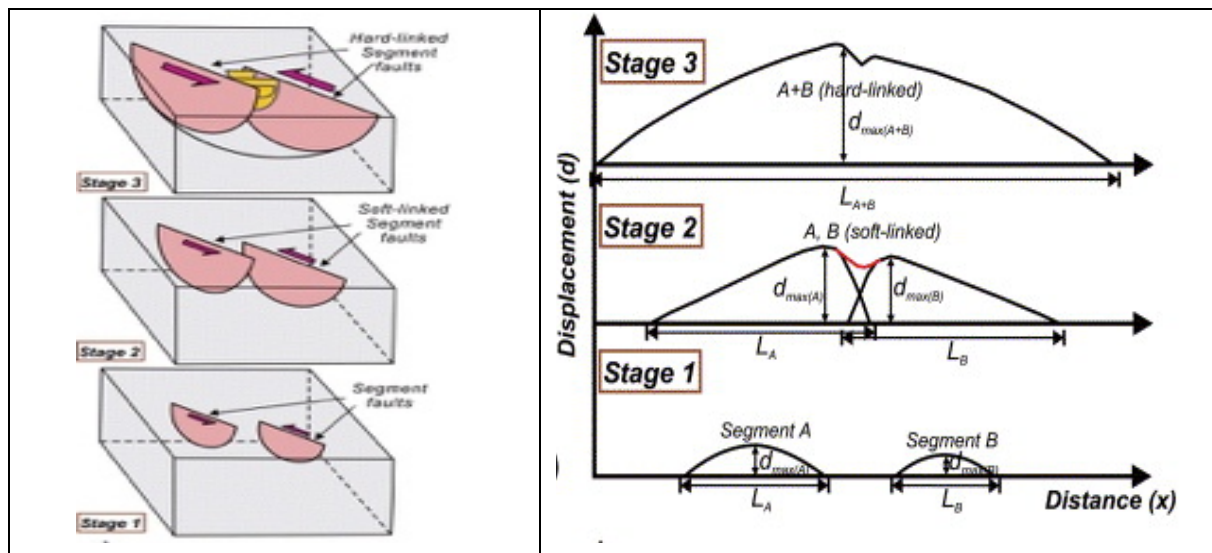
Figure 2.6: a) shows three stages of fault growth. Stage 1 is two isolated fault segments growing, Stage 2 shows how the two fault segments overlapping and soft-linked, Stage 3 shows the two fault segments when they are hard-linked. b) Shows a displacement-distance diagram and illustrate the same stage for the fault segments in figure a). From (Kim & Sanderson, 2005)

These intersection points are categorised based on its geometry how the intersection occur. The abutting pattern (Fig. 2.7a) is described as a fault propagates towards a second fault and interact. The abutting fault have only opportunity to propagate in the opposite direction with the isolated fault tip (Fig 2.8) (Nixon et al., 2014). A splaying pattern (Fig 2.7b) occur when a new fault tip starts to propagate from an existing fault. These two terms for pattern can be used for several other description in a fault network.

16
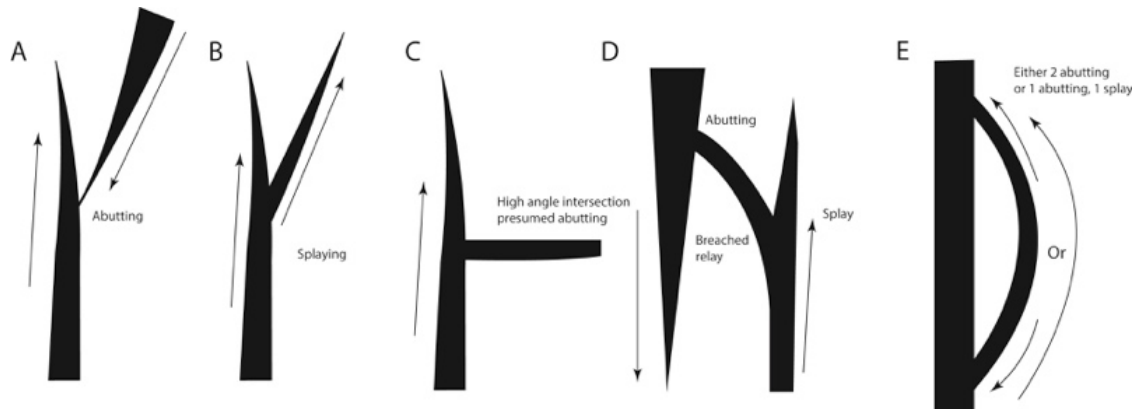
Figure 2.7: illustrate different type of intersection that occur and the fault pattern in the surface. From (Nixon et al., 2014).
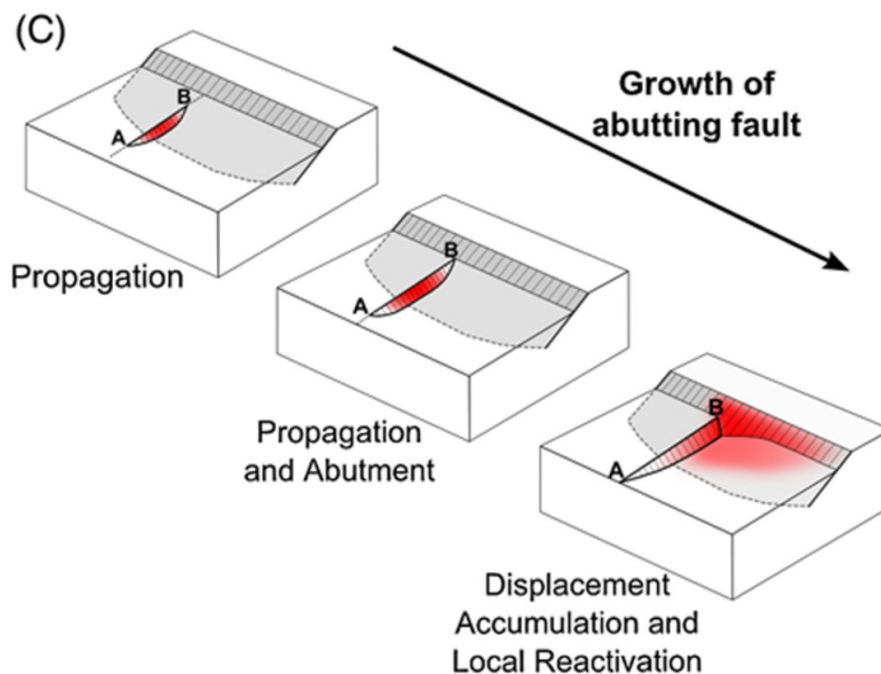
Figure 2.8: shows how an already existing fault can control the propagation of a second fault From (Nixon et al., 2014)

Stress affects the growth pattern to fault segments. Around a normal fault is the stress distribution located in different zones (Fig. 2.9). The stress is at its highest at the fault tip (Fig. 2.9) and this region accommodates multiple microfracture. These fracture weakens the rock and influence the fault to grow in their favourable direction (Fossen, 2016). Along the fault plane reduces the stress further away from the fault plane (Fig. 2.9). If a second fault (Fig. 2.9 Fault 2) enters the stress drop zone of the first fault (Fig. 2.9 Fault 1), the propagation of the fault is retarded.
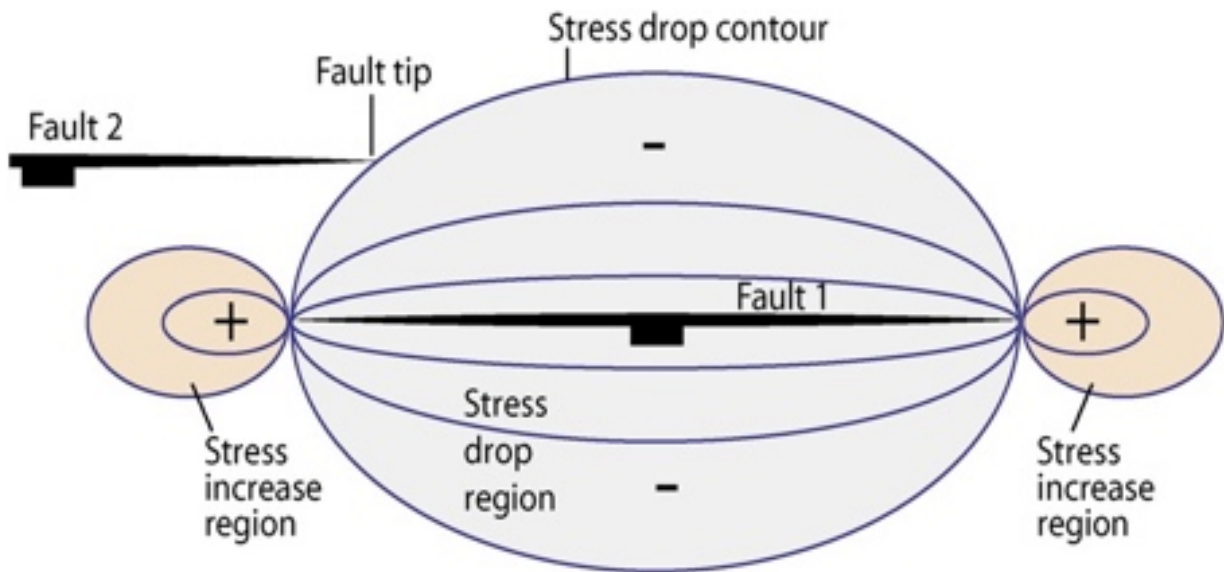
Figure 2.9: Shows the distribution of stress around a normal fault. From (Fossen & Rotevatn, 2016)

2.3 Relay ramp

A relay ramp is presented as overlapping or underlapping sub-parallel faults segments in a zone of kinematic linkage (Peacock et al., 2016). They are geometrically uncoupled, with a ramp separating the fault segments (Fig. 2.10a). Relay ramps occur in all scales and settings and acts as a coherent system (Fossen & Rotevatn, 2016). Ramp geometry includes the shape of the ramp and the variation of the displacement present in the overlapping tips of the faults (Fossen & Rotevatn, 2016).
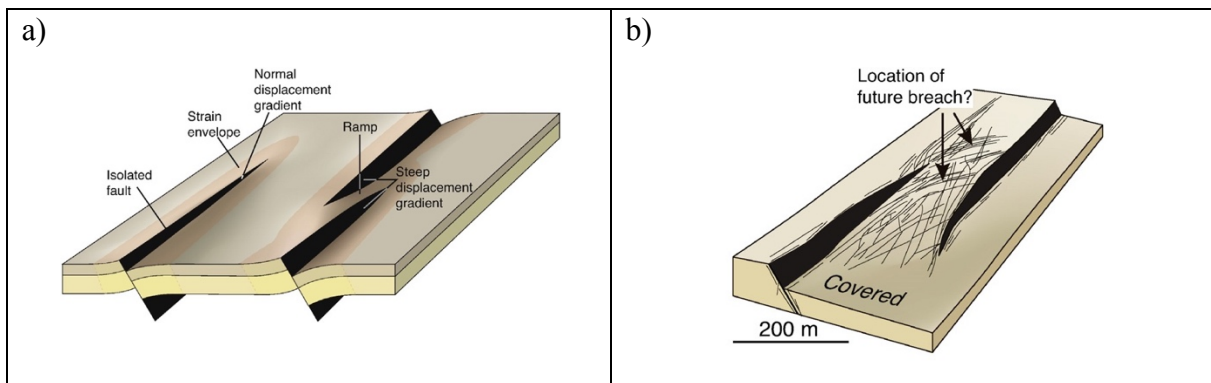
Figure 2.10: a) shows an illustration of an isolated fault and a relay ramp structure. From (Fossen & Rotevatn, 2016) b) Shows an illustration of a relay ramp with several fracture. Can these fractures indicate occurrence in the future? From (Fossen & Rotevatn, 2016)

Peacock and Sanderson (1991,1994) introduced four stages for the evolution of relay ramps regarding the deformation and displacement. The first stage (1) represents the isolated fault with no overlapping or interaction to other faults. In the second stage (2), faults propagate and start to interact through ductile strain, presenting soft-linked fault segments that create the relay ramp structure. The third stage (3) is characterized by fractures across the relay ramp (Fig. 2.10) causing the two fault segments to link. Several factors as strain, the availability of faults and their distribution and arrangements etc. controls the linkage and breaching of a relay ramp (Fossen & Rotevatn, 2016). The last stage (4) represent the breaching of the relay ramp and is divided in to three classes based on where the relay ramp breaches (Fig. 2.11) (Fossen & Rotevatn, 2016). The single-tip breach (b), where one of the faults tip curves towards the other and link the fault segments together. The ramp is then preserved in the hanging wall or the footwall. The second is a double breached (c) relay ramp and represent when both of the fault segments curving towards each other and both of the fault segments tips link together. In this case will a 'lens' be preserved in the slip surface. The third is a mid-ramp breach (d), where it breaches between the two faults and links them together.
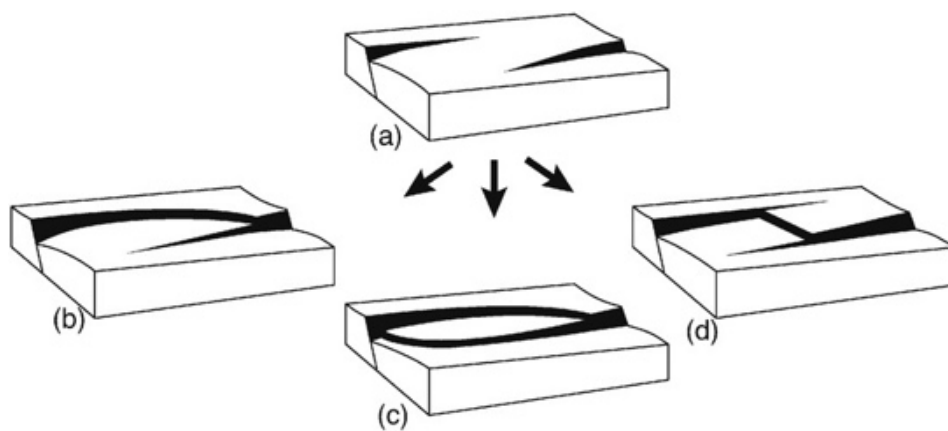
Figure 2.11: illustrate a relay ramp (a) and potential ways to breach (b) a single-tip breach, (c) a double breach and (d) Mid-ramp breach. From (Fossen & Rotevatn, 2016)

Rheology and mechanical layer properties and kinematic boundary controls the arrangement of faults in the population (Fossen and Rotevatn, 2016). The arrangement of faults is essential together with density and distribution for the accessibilities for faults to linkage (Fossen and Rotevatn, 2016). Fault segments start to interact if the faults are close enough. If the fault tip propagates into the stress drop region to an overlapping fault, the fault-tip will start to curve, propagating towards the stress drop zone (Fig. 2.9) (Fossen & Rotevatn, 2016).

CHAPTER 3 – THEORETICAL BACKGROUND

3.1 Introduction

The aim of this chapter is to provide an overview of previous analogue experiments and present terminology and theory related to fault growth and the topology in an extensional regime.

3.2 Theoretical background of analogue modelling

3.2.1 Pioneering modelling work in the 1800´s

Execution of different type of analogue models have been experimented with over several decades. Hall (1815) performed the first documented experiment (Graveleau et al., 2012). He took an interest in the folds that he observed in the east coast of Scotland and wanted to understand how these were formed. Clothing was used to illustrate different layers and a heavier material put on top of the clothes to control the vertical movement. To perform the experiment, he had two wooden boards on each side of the clothes. He used them to push the layers towards each other in horizontal direction. With this experiment he achieved to form a compressional regime and fold structures (Graveleau et al., 2012).
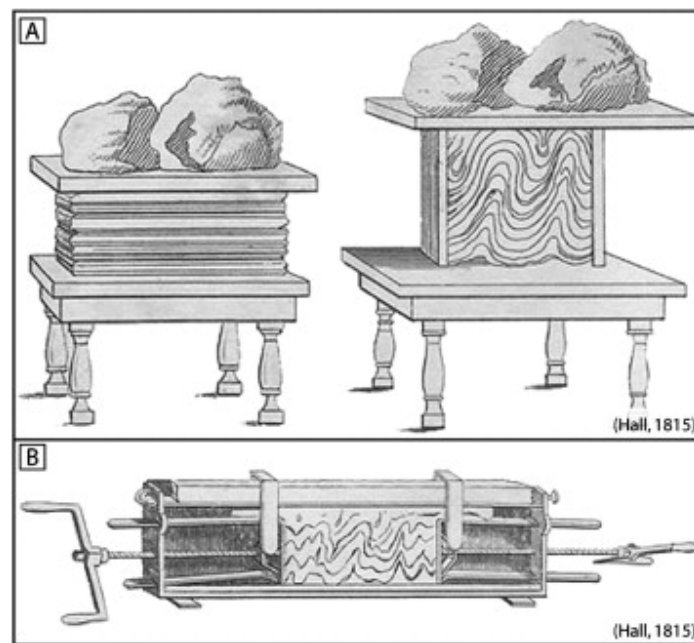
Figure 4.3: a and b shows Hall (1815) first experiment setup. From (Graveleau et al., 2012)

Several pioneering modeling work of various complex geological events and structures were carried out in the period after. Some of the experiments performed were to investigate rheology and pressures performed on a single layer (A. Daubrée, 1879; G. A. Daubrée, 1878), also study how anticlinal and synclinal structures are formed (Favre, 1878) and some experiments to explore how mountains are formed and the structures that occur in compressional environment (Cadell & Edinburgh, 1889; Willis, 1894).

In the middle of the 1900s was hydrocarbons found traps in structures that occurred in an extensional regime. This increased the interest of studying extensional faults by using different types of experiment that showed how these faults were formed and grew. At the same time as knowing what controlled these structures and which patterns they formed (E. Cloos, 1981; W. J. F. T. i. N. E. Horsfield, 1977; W. J. J. o. S. G. Horsfield, 1980; Mandl, 1988).

Various type of material has been used to find a product that is comparable to how different geological events occur. Some of the different materials used are plaster (Fossen & Gabrielsen, 1996; Lindanger et al., 2004; Mansfield & Cartwright, 2001; Sales, 1987), sand (Hus et al., 2005; McClay & Ellis, 1987; McClay & Scott, 1991), clay (Ackermann et al., 2001; E. J. G. S. o. A. B. Cloos, 1955; Henza et al., 2010) and several other material as zinc, iron, lead rubber, wax, oil, honey putty etc. (A. Daubrée, 1879; G. A. Daubrée, 1878; Favre, 1878),

3.2.2 Analogue plaster modelling

Plaster have been used by Sales (1987) for analogue models for an extensional regime. Fossen and Gabrielsen (1996) used it in an extensional fault system experiment to study lense-shape geometry and small-scaled structures in relation to larger fault system.

Mansfield and Cartwright (2001) used plaster in an experiment that shows a good overview over the experiments surface and show how the faults grow. This gives an opportunity to describe how fault grow. They studied mainly the accumulation of displacement and how the fault lengthening. This is the same experiment used in this thesis.

3.3 Scaling

King Hubbert (1937) described three criteria that needed to take place in an analogue experimental model for giving it the right dimensional to compare it to a process in the nature.

- The two bodies need to be geometrically similar. This is obtained if the two bodies correspond proportional in lengths and angles (Hubbert, 1937).
- The two bodies need to be kinematically similar. This is achieved when the two bodies share the same change in shape and/or position. Also, the motion in the bodies need to have a constant time ratio (Koyi, 1997).
- The two bodies need to be dynamically similar. This is completed when the force acting on the two bodies is constant for all the particles in the bodies (Koyi, 1997).

Hubbert (1937) found that a given material in a small body are stronger than larger body with the same material and that the body weakens with a larger size. This means that the strength and size of a body needs to be considered before it is used to perform an analogue model to get it most possible perfect to compare to the nature. Hubbert (1937) also found that if the pressure increases in the material, its strength will increase as well. Also, if the temperature increased in the body will the strength decrease.

3.4 Fault growth model

The normal fault growth is investigated by exploring the relationship between length and displacement (Cowie & Scholz, 1992a, 1992b; J. J. Walsh & Watterson, 1988; Watterson, 1986). Studies have documented that the displacement of the fault is zero at the fault tip and increases to a maximum close to the centre of the fault plane (Watterson, 1986) , but it is also known that the displacement varies in the fault plane (Barnett et al., 1987). The evolution of the fault growth is researched by investigated the fault propagation and the history of slip (Cowie & Scholz, 1992a, 1992b; Peacock & Sanderson, 1996; J. J. Walsh & Watterson, 1988). The fault growth by displacement accruing is often associated with earthquake (Dawers & Anders, 1995; J. Walsh et al., 2002)

The first recognized fault growth model was referred to as the 'isolated fault model' and was first described as kinematic independent segment propagating and by accident overlap, interact and forms a relay ramp (Cartwright et al., 1995; J. Walsh et al., 2003). An alternative model was provided by J. Walsh et al. (2002) called 'coherent fault model'. He suggested that the fault lengthens rapidly and established it near final length before entering displacement accrual. These two fault growth models have got new terms the 'propagating' fault model have replaced the 'isolated fault growth, and is described as synchronously growth between length and displacement, and the 'constant-length' fault growth model have replaced the term 'coherent fault model' (Rotevatn et al., 2018). These models are described further in chapter 2.

CHAPTER 4 – METHODOLOGY

4.1 Introduction

The aim of this chapter is to provide a detailed description of the method used for this project, i.e. analog modeling of an extensional regime.

The set-up of the experiment is demonstrated and the performance and the various of material are explained. At the end of the chapter there is a small summary of why this type of method can provide limited information associated with natural structures

4.2 Set-up and performance

The experimental setup is similar to that Mansfield and Cartwright (2001) used in their paper, but there is a small difference between the measurements in width and height (Fig. 4.1). This is an open top wooden box with a moveable internal wall. The execution of the experiment starts when the handle attached to the moveable wall is rotated. This sequence creates an extensional regime by stretching the plaster (Fig. 4.1).
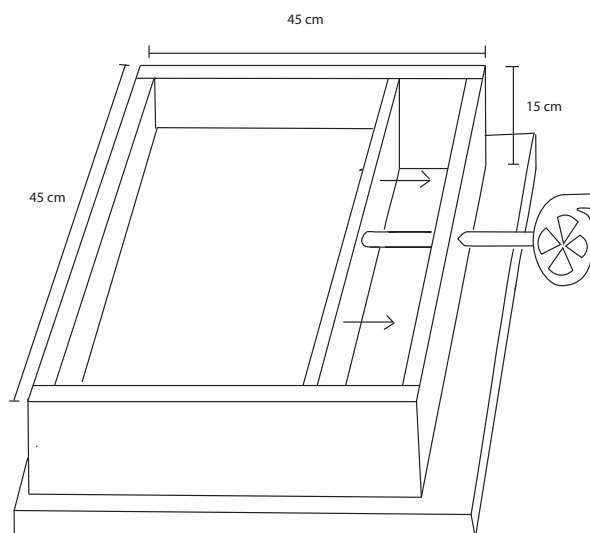

Figure 4.1: illustrate the experimental box used to perform the analogue models. The handle is attached to an adjustable wall which makes it possible to control the extensional stretching in the plaster. Modified from (Mansfield & Cartwright, 2001)

The material used to perform the experiment are plaster of Paris, barite and canola oil. The canola oil is lubricated over all the side walls of the experiment to reduce the friction between the wooden walls and the plaster. The first layer in the experiment is the barite and is used as a basal layer for the plaster. The barite also seals the experimental box and prevents it from leaking during the experiment. The first two experiments feature a horizontal layer of barite and the last two experiment has the barite a wedge shape.

The last material added to the experimental box before it starts is the plaster of Paris. The rheology of the plaster is very ductile when it is added and needs to settle before the experiment can start. A screw is used to determine that the rheology of the plaster is sufficient to start the experiment by making a pile on the surface, if the plaster retains the pile it forms for a short period of time it would establish that the plaster is settled.

When the experiment starts, and the movable wall extends, extensional structures will start to breach the surface of the plaster.

To highlight structure and details on the model, four different light sources are used. Two lamps were attached to the wall and two lamps were handheld throughout the experiment. The cameras are started manually when the experiment begins and documents the deformation that appears in the plaster. This makes it possible to follow the whole growth history of the structures in the models.

4.3 Plaster of Paris

Plaster of Paris is the main material in the experiment and contain the structure to be studied in this project. Plaster is beneficial to use in this experiment because it gives a good overview of small-scale structures and how these structures occur and evolve. The plaster used in this project is `Molda 3 normal` and consist of a high purity gypsum mineral and is a hemihydrate plaster ($CaSO_4 * \frac{1}{2} H_2O$)(Saint-Gobain, 2019). The plaster consists of at least 91% pure gypsum and have a white color. 97% of the grains exhibit a size less than 100μ, and the rest fall between 100-200μm (Saint-Gobain, 2019). The rheology of plaster is determined by the water and plaster ratio and the temperature on the mixture. These factors control when the plaster have the right rheology to start the experiment and the time needed for the plaster to solidify.

All of the experiments in this project have the same mixture of water and plaster. The water temperature was kept constant between experiments. The ratio between the water and plaster is 1.7:1. The plaster used 39 minutes from the point where it was added to the experimental box before it was completely solidified (Saint-Gobain, 2019). The models are then preserved to be used for analysis at a later occasion.

Sales (1987) alleged that it is not possible to achieve a dynamically similar analogue model to a natural example. But plaster is the preferred method to study normal fault growth because it is similar to those observed in naturally extended crust (Fossen & Gabrielsen, 1996).

Fossen and Gabrielsen (1996) found that 1cm in the plaster model represent 0.1-1 km in the nature.

4.4 Basal layer

All the experiments performed have a basal layer to give the plaster a surface to glide on and to shape a relief (Fossen, 1995). It was used to investigate whether different basement configurations give different extension result on the surface.

The basal layer used is barite ($BaSO_4$) mixed with water, which has been used in previous plaster modelling studies (Fossen & Gabrielsen, 1996; Mansfield & Cartwright, 2001; Sales, 1987) The barite has a higher viscosity than the plaster. It deforms in a ductile manner and will not solidify to the plaster (Fossen, 1995). Two of the experiments (1 and 2) feature a horizontal layer of barite, whereas two of the experiments (3 and 4, Fig. 4.1) feature a wedge-shaped layer of barite.

Experiment 3	Experiment 4
a)	b)
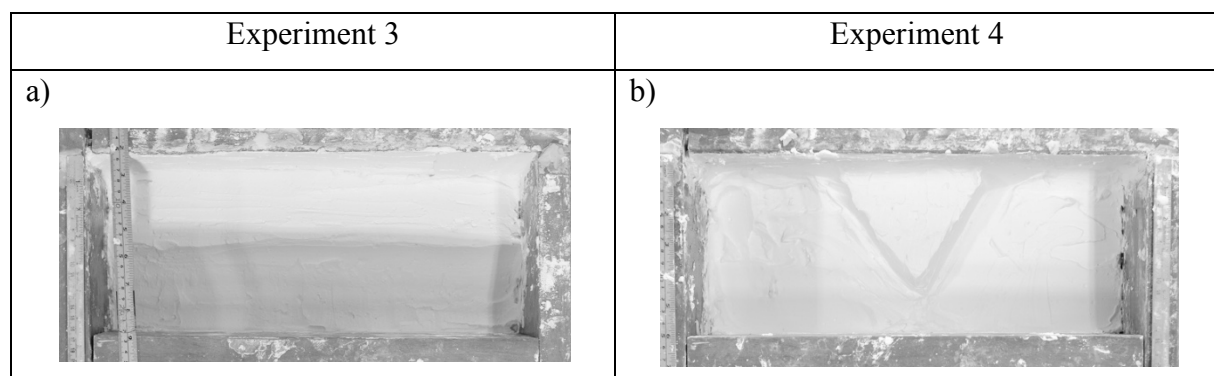
Figure 4.2: shows how the barite layer is formed for the two experiment with a wedge-shape, a) Experiment 3 and b) experiment 4.

4.5 Documentation

To document the experiment, three different cameras are used. They are placed to capture the experiment from different angles and perspectives. One of the cameras is placed in front, one is placed on the side, and the last one is placed directly above the experimental box. The cameras are manually but remotely controlled. The cameras used for these experiments are high-resolution cameras (Nikon D800). All three cameras had an AF-S Nikkor 50 mm f/1.4G lens. The resolution used on the cameras is 7360*4912 pixels. This gives the opportunity to get a good overview of small-scale structure for each experiment. Each camera takes 4 pictures per second during the experiment run.

The experimental box is equipped with two rulers on both side parallel to the extension direction for all the experiments. These rulers are included in all of the images for scale, and they also contain information about the time and date for each image taken.

4.6 Collecting and processing data

The images documenting the experiment are essentially what is used to extract information and interpret each of the experiments. All of the images were edited in iPhoto (Mac) to elucidate the important details and prepared to be analysed in Adobe illustrator.

Adobe illustrator is a program that design physical quantity with vectors. For this project is this program used to extract information and measurements from all the images in the different experiments and to create maps and figures.

4.6.1 Amount of extension

A stepwise description of each experiment is distributed with percentage extension. Each step is selected based on the image that describe the evolvement in the model in the best way.

This formula was used to calculate the extension percentage for each timesteps of the analogue models:

$$\varepsilon = \frac{(l - lo)}{lo} \times 100\%$$

ε = Amount of extension in %

l = Amount of extension in mm/extended model length

lo = Initial length in mm

The initial length is measured when the plaster is filled into the experiment box before the experiment starts. The amount of extension is measured for each step selected to describe the experiment. If the amount of extension is twice as long as the initial extension length, the experiment has prolonged by 100%.

To find the rate of extension for each of the experiments used the following formula:

$$\dot{\varepsilon} = \frac{\varepsilon}{t}$$

$\dot{\varepsilon}$ = average extension rate (mm/s)

ε = Extension length (mm)

t = time (seconds)

The average extension time is found by measuring the extension length and extracting the information about the time of the desired attempt

4.6.2 Length and heave

All important and visible faults in the analogue model have been analysed in this project. Two measurements per seconds have been extracted for the length and heave from images of main faults, fault segments and sub-segments to be plotted in to the displacement-length diagram. The length is found by measure along the faults trace length and heave is proxy for displacement and is consequently used for all measurement in this project (Fig. 4.1).

4.7 Limitations for this method

Analogue modelling provides very good results compared to occurrences in nature, but there are still some disadvantages by using this method. The same experiment box is used for all experiments, yet there are several possibilities for it to be able to influence the outcome of the experiments.

- The internal movable wall moves unevenly as the wall itself is not completely fixed to the handle.
- The internal wall is also determined from the speed of the person who carries out the experiment and does not necessarily become the same for each experiment.
- When the experiment starts, the rheology of the plaster is determined by a screw. The plasters rheology and when to start the experiment is only determined from å subjective viewpoint and not an exact measurement.
- A frictional drag occurs between the plaster and the sidewall and can affect the flow and deformation in the plaster.
- The plaster mixture solidifies during the experiment and changes rheology of the plaster throughout the extensional process. This makes it difficult to quantify the properties plaster (Fossen & Gabrielsen, 1996).
- Water is released from the plaster along the way and deposited on the surface. This water erodes the structures that forms and can make it difficult to interpret the results.
- Air bubbles appears in the surface of the plaster. These can control how the structure shows on the surface, and perhaps the ability to control how the structure grows.

- The plaster is a homogenous material and gives the best example for a smaller scale structure (Fossen & Gabrielsen, 1996). The larger scale rocks in nature usually have a natural bedding that the experiment does not take in to account.
- all the structures are measured in millimetres and are interpreted from a subjective point of view.

CHAPTER 5 – RESULTS

5.1 Introduction

This chapter describes four plaster experiment that emulates crustal extension. All of the experiment is produced in the same experimental box and documented using three different cameras. Images are used to give a stepwise documentation of the models in time and percentage extension.

General information about each experiment is provided in tabularized format (Table 5.1). *Initial length* is the pre-kinematic length of the experiment, i.e. the length between the outer (north) wall and the moveable wall where the plaster is added. *Final length* is the post-kinematic length of the experiment, i.e. the length between the outer (northern) wall and the movable wall after extension has ended. *Total displacement* is the difference between initial length and final length. *Total extension* (also see Ch. 4 – Methodology) is the extension of the experiment in percentage. The initial length is then described as 0 % extension and the final length are 100 % extension.

Each of the experiments are divided into timestep from T1 to T5 and is described with time and extension. The timesteps are determined by the events that occurs in the experiment and pictures that gives the most information about the processes and events.

The segments are divided in to three levels. A main fault is described with capital *F*, for example *F1* for the first main fault. The precursor and/or subordinate segments of a fault F are denominated *S* for segment. For example, S1, S2 etc. may grow and link to become F1. Some of these are also described in smaller sub-segments, in which case they are referred to as S1a, S1b, etc. (Fig. 5.1)
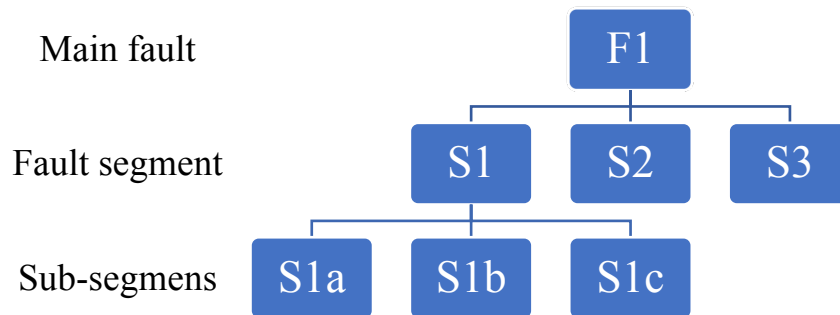
Figure 5.4: illustrate the levels the (main) fault are divided into and how they are connected

Two displacement-length (D-L) diagrams are shown for each experiment. They show the growth trajectory in D-L space for several of the segments in each experiments. The first diagram shows the linking of the main fault and the second diagram shows the growth of segments outside the proximity of the main fault.

5.2 Description of experiment 1

Table 5.1: General information about experiment 1

Date	14.10.2015
Plaster to water ratio	1:1.7
Basal layer	Horizontal
Initial length (mm)	151
Final length (mm)	285
Total displacement (mm)	134
Total extension (%)	88,7
Duration (second)	24
Mean extension rate (mm/s)	11,9
Notes	

General information of the evolving of the experiment

From start to timestep T1

Sub-segments of S1 and segments S2, nucleate and breach the surface after 5 seconds and 17 % extension (Fig. 5.2a). They lengthen in east-west direction, perpendicular to the extension direction and the displacement to the segments is close to zero.

Segment S1 grows in the eastern part of the model and segment S2 grows in the middle of the model (Fig 5.2 a-b).

Segment S1 evolves from several isolated sub-segments that link by their segment tips (Fig. 5.2 a-b). Segment S2 reaches over a larger area and is the first fault to accrue displacement, after 7 seconds and 21 % extension. The length of Segment S2 is 50 mm and the heave are 4 mm at T1 (Fig. 5.2 a-b).

<u>T1 to T2 – 21.9-30 %:</u>

Segment S1 has grown by smaller sub-segments that propagated and linked together by the segment-tips (Fig. 5.2 c-d). The fault nearest to the movable wall (south) has curved northwards and linked together with the fault to the north.

Segment S2 has grown by segments propagating in length direction and linked with a segment to the west of it (Fig. 5.2 c-d). Segment S2 features a length of 121mm and a heave of 9 mm at T2.

Sub-segments of S3 have nucleated and started growing at T2 (Fig 5.2 b-c).

S1, S2 and S3 are separated by multiple relay ramps. The relay ramp (R1) separating S1 and S2 has the widest spacing between S1 and S2 (Fig. 5.1 c-d). Small fractures occur in the middle and upper part of the ramp.

Segment S2 and S3 overlap each other developing relay ramp (R2).

<u>T2 to T3 – 30-40 %:</u>

In the northern part of the experiment nucleates segment S6 after 30 % extension (Fig 4.2 e-f). It reaches its full length after 40 % extension and subsequently accrues displacement without further lengthening.

Relay ramp R1 breaches after 31 % extension by segment S2 splaying in the lower part in the west of the segment.

New smaller segments nucleate after 8 seconds and 32.5 % extension near the east and the west wall in the middle of the experiment in the same direction as S1-S3.

Relay ramp R2 breaches as the eastern tip of segment S3 propagates eastward in the lower part of R2 and curves northward towards segment S2. R2 breaches after 35.7 % extension and accrue a displacement (Fig 5.2 e-f).

A relay ramp to the west in the experiment (not marked in Figure 5.2) breaches by fracturing in the middle part of ramp after 10 seconds and 37.3 % extension. All the segments S1-S3 are fully linked to comprise the main fault F1, extending east-west across the experiment (Fig. 5.2 e-f). This is shown in the displacement vs. length (D-L) diagram (Fig. 5.3) where several segments exhibit a very steep D-L curve.

At T3 are the maximum heave of the main fault F1 measured to 16 mm at the location of S2 (Fig. 5.2).

T3 to T4 – 40-69.5 %

Segment S6 stops accruing a displacement and stops growing after 50 % extension.
After ~ 60 % extension nucleates new segments in the hanging wall of the main fault F1.
Sub-segments of S4 is located to the east. The sub-segments to the west propagate in a
northwest-southeast direction, while the other segment propagates in northeast-southwest
direction towards the other segment (Fig. 5.2 g-h).
Sub-segments of S5 is growing from the center of the hanging wall and transverse
overlapping each other towards west direction. The segments lengthen mainly in an east-west
direction (Fig. 5.2 g-h).

T4 to T5 – 69.5-78.1 %:

The sub-segments of S4 are connected by the segment propagating towards the middle of sub-
segment links and it stops growing, creating an abutting pattern at ~72 % extension.
After ~ 78.1 % extension and 24 seconds has F1 reached its full maximum heave at 33 mm.
Segments S5 and surrounding segments lengthen between T4 and T5 and several of these
segments' curves at the east of the segment-tip and grow northwards to link with the segment
in the north of itself (Fig. 5.2 g-h).

Fault segment behaviours in D-L space

Plotting the above described segments as well as all smaller segments in the experiments in D-L space (Fig. 5.3 and 5.4) shows that almost all of the segments in this experiment exhibit elements of staged growth , exhibiting (i) lengthening with minimal displacement accumulation, before (ii) entering a stage of displacement accrual and limited lengthening, which in turn is followed by (iii) renewed lengthening and low-rate displacement accumulation in concert. Another stage (iv) is seen upon linkage and assembly of F1, which is arrested (by the walls) when it reaches 400 mm in length. After this, displacement accrual continues to the end of the experiment.

The first diagram (Fig. 5.3) Shows that segments start accruing a displacement between 10- and 40-mm. Segment S3b has the smallest length before accruing a displacement with the length ~10 mm, and segment S3c is the longest before accruing a displacement ~40 mm. Segments S2a is the only measured segment that start to grow both in length and displacement from the start.

The second diagram (Fig. 5.4) shows segments growing proximity of F1. It shows the growth in a smaller scale, since these segments are smaller. The first segments measured start to accrue a displacement after lengthening 12 mm and the last segments lengthens 24 mm before accruing a displacement (Fig. 5.4).
A closer look at the details of these diagrams shows that the segments grow in several periods in length and displacement.
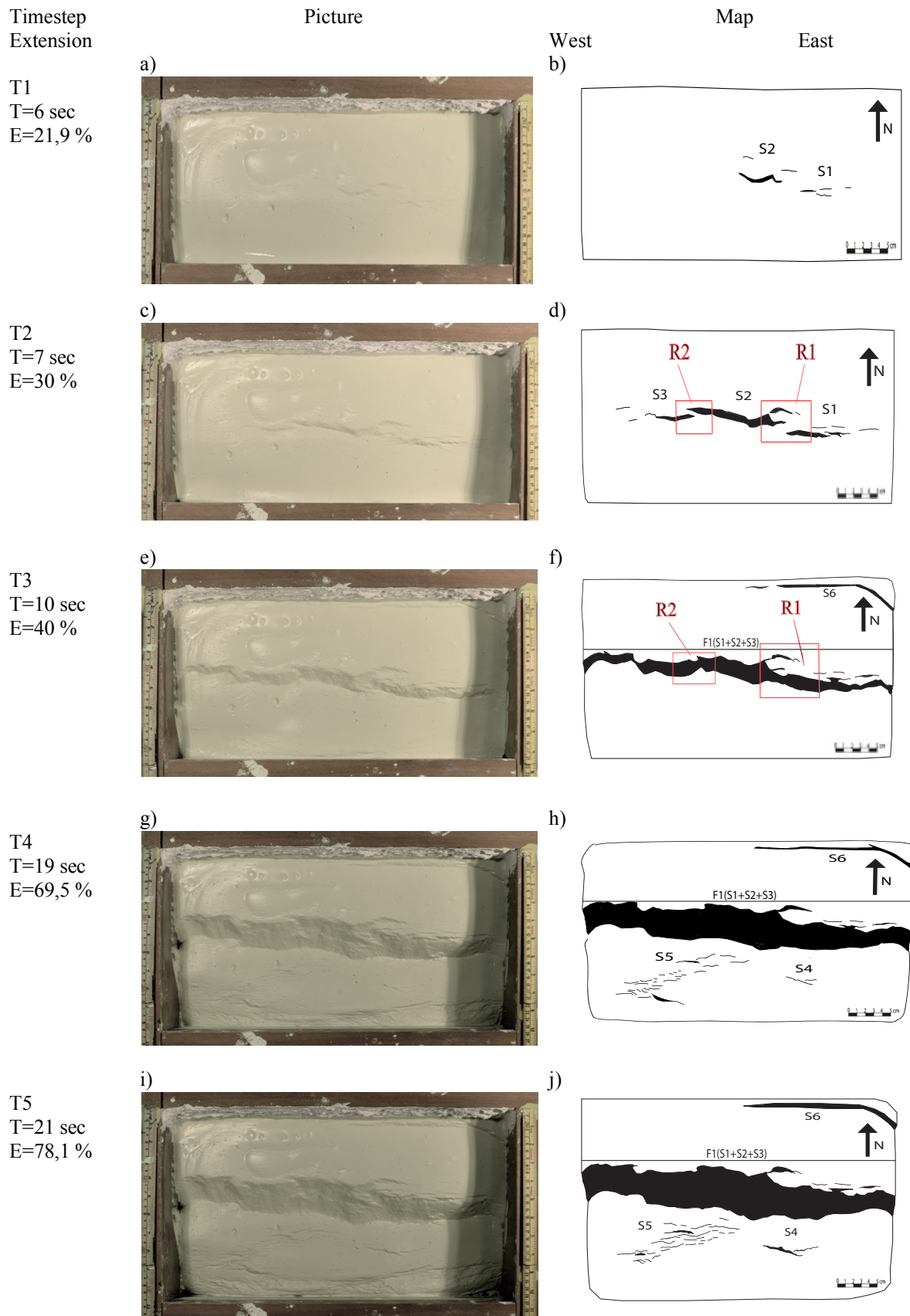
Figure 5.2: shows the evolution of an extensional regime in a plaster experiment. It is divided in to five timesteps (T1-T2) that accentuate the deformation that occur. The picture to the left shows the plaster model at given time and extension. To the right is an overview map of the deformation occurring in the picture beside. The moveable wall is to the south
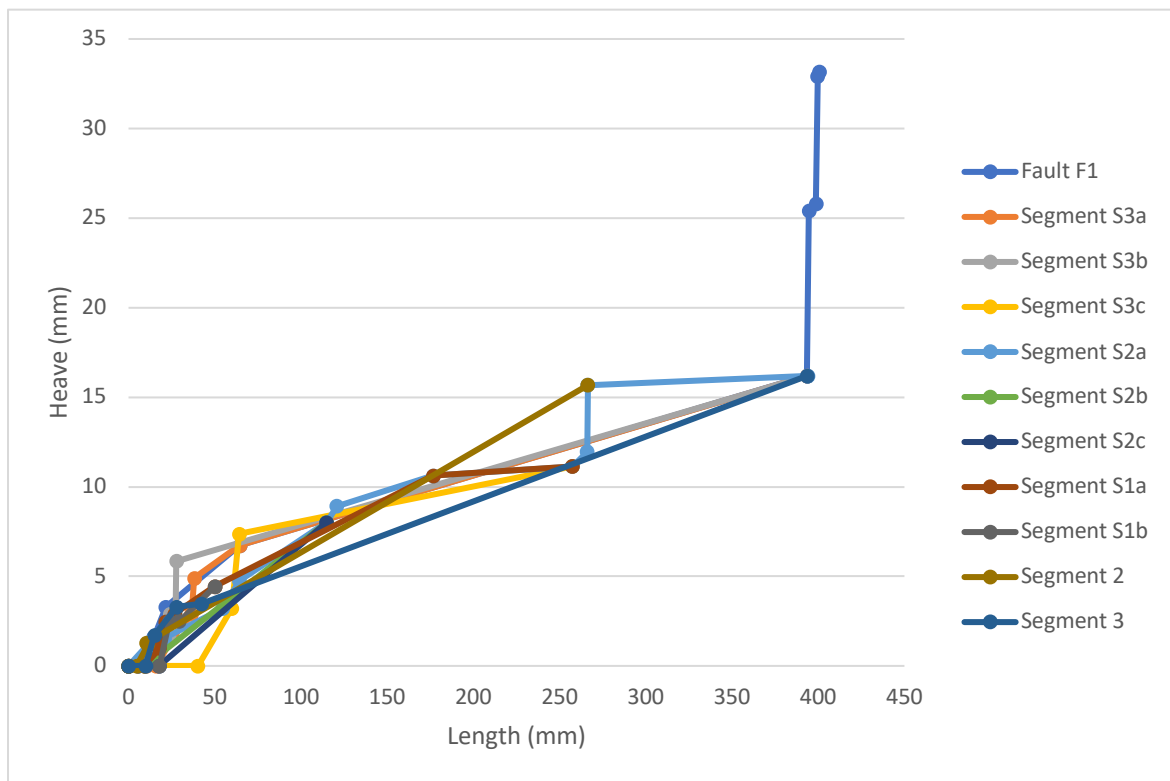
Figure 5.3: shows faults and fault segments related to the growth and assembly of fault F1. Note that upon arrest of the tips at the experiment boundary the fault stops to lengthen and then accrues displacement (Fault F1).
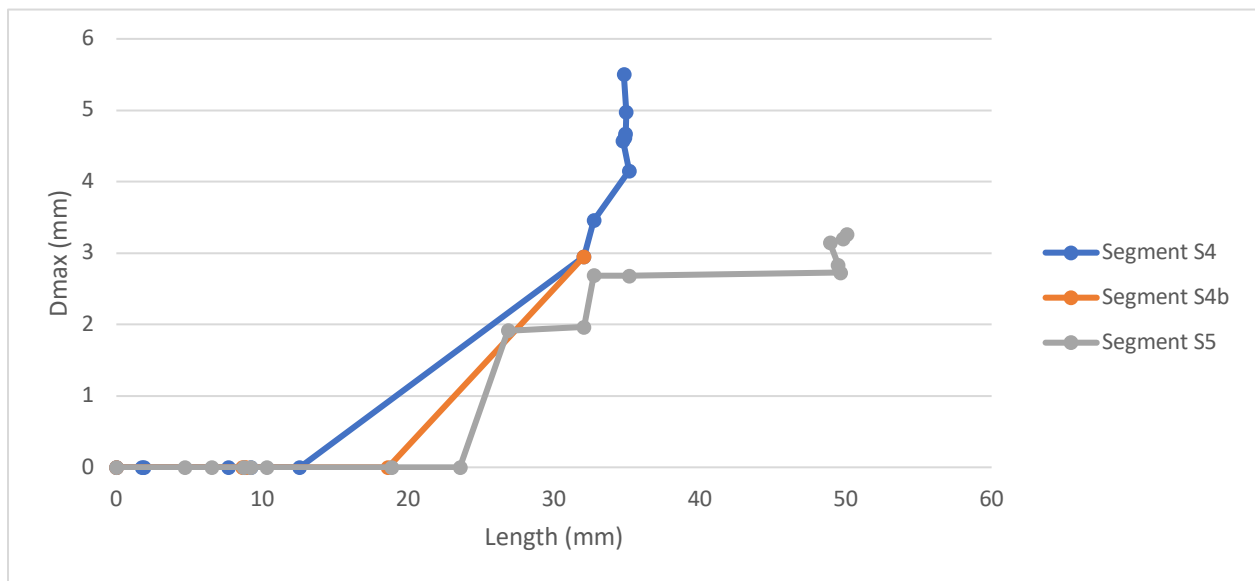
Figure 5.4: showing all measured segments that occur outside the proximity of F1.

5.3 Description of experiment 2

Table 2: General information about experiment 2

Date	30.10.2015
Plaster to water ratio	1:1.7
Basal layer	Horizontal
Initial length (mm)	168
Final length (mm)	280
Total displacement (mm)	11
Total extension (%)	66.7
Duration (s)	46
Mean extension rate (mm/s)	6.1
Notes	A volume loss during the experiment was approximately 50.4 cm^3.

General information of the evolving of the experiment

From start to timestep T1 – 0-23,8 %

After ~12 seconds and 23.2 % extension nucleate the first segment through the surface of the plaster. They grow mainly in an east-west direction perpendicular to the extensional direction (Fig. 5.5 a-b).

Fault segments S1 is located in the west part of the model (Fig. 5.5 a-b). Mainly two segments, one with a northeast direction and one approaching the first segment with the tip on the westside propagating straight towards it

Fault segment S2 is two segments approaching one another with the segment tips straight towards each other (Fig. 5.5 a-b).

Fault segment S3 are at this timestep three small segment overlapping each other and is soft-linked and creating relay zones (Fig. 5.5 a-b).

Fault segment S4 is several segments overlapping each other transverse toward east direction (Fig. 5.5 a-b).

<u>T1 to T2 – 23.8-28 %</u>

After 25 % extension and 14 seconds starts the first segment to accruing a displacement and the last segment to accruing a displacement at 28 % extension.

At T2 (Fig. 5.5 c-d) has several new nucleates and already existing segments have propagated and some have linked since T1.

Segment S1 shows how the two segments have linked. The segment to the west propagates and link together in the middle of the segment to the west and developed an abutting pattern.

Segments S2 propagates and linked together by the segments tip. Segment S2 have then propagated both at the east and west side (Fig. 5.5 c-d) and started accruing a displacement. Several new segments nucleated between segment S2 and S3. These have propagating in length direction and accruing a displacement.

Segment S3 are overlapping each other creating a relay ramp (Fig. 5.5 c-d).

In location of fault segment S4 have segments grown and linked, creating three larger fault segments separated by soft-linked relay ramps. All the fault segments (S1-S4) define a dominant segment trend through the middle part of the model and are separated by soft-linked relay zones.

<u>T2 to T3 – 28-33.3 %</u>

At 29 % extension and 17 seconds an increase in slip rates occur in the experiment and segments enter into a stage of significant displacement accrual. This is shown in the displacement vs. length (D-L) diagram (Fig. 5.6) where several segments exhibit a very steep D-L curve.

The relay ramp between segment S1 and S2 breaches by segment S2 propagates westward and linking in the mid part of segment S1 (Fig. 5.5 e-f).

The relay ramp between segment S2 and S3 breaches in the middle of the ramp, arresting the segment tip to both segment S2 and S3 (Fig. 5.5 e-f).

The relay ramp between segment S3 and S4 breaches by the segments to the east propagates northwards and through the lower part of the ramp. Also, some breaches in the upper part, creating lenses in the displacement plane (Fig. 5.5 e-f).

After 21 seconds and 33 % extension are all the fault segments (S1-S4) linked together creating a fully linked fault (F1) from the east wall to the west wall (Fig. 5.5 e-f). This is shown in the displacement vs. length (D-L) diagram (Fig. 5.6) where all segments are linked

and only accruing a displacement. At T3 is the F1 maximum heave measured to be 11 mm
and is located where S3 was created (Fig 5.5 f).

A second stage of increased displacement accrual occurs when F1 reaches its full length. It
went from ~1 mm/sec to 2 mm/sec.

At the same extension and time several new segments nucleate in the hanging wall of F1
(32.7 %).

Fault segment S5 and S6 nucleate with an east-west direction (Fig. 5.5 e-f). Fault segment S5
is comprised of two approaching segments and one of them is overlapping the last segments
with soft-linkage (Fig. 5.5 e-f). Segment S6 is an isolated segment.

T3 to T4 – 33.3-38.1 %

Segment F1 continues to accrue a displacement, and at T4 is the heave measured to be 18 mm
(Figure 5.6). Several new segments have nucleated in the hanging wall of F1 at T4.

The sub-segments of S5 links at 35 % extension, and S5 subsequently initiates a stage of
significant displacement accrual at 37.5 % extension.

Segment S6 are the first segment to accrue a displacement of all segments in the hanging
wall. This occurs when the model has reached 37 % extension.

New segments (S7) nucleate between S5 and S6 after 36.3 %. They grow in the same
direction as S5 and S6, parallel to the movable wall with an east-west orientation.

T4 to T5 – 38.1-48.2 %:

The maximum heave of Segment F1 is 41 mm at ~ 60 % extension and 40 second, measured
where segment S2 were located (Fig. 5.5 j)

Segment S7 and S6 propagates towards each other and links together by the tips.

Segment S5 and S7 overlap each other. Segment S7 overlaps from the north and propagates
southwards and link together with segment S5 to the south.

As the extension proceeds are segment S5 still active and its segment tip propagate towards
the segment to the north, linking the segments a second time together, creating a double-tip
breached ramp.

All segments S5-S7 are fully linked together after ~ 43 % extension and develops the major
fault (F2) (Fig. 5.5 i-j).

F2 is 175 mm in length and 4mm in maximum heave when all the segments S5-S7 are fully
linked. This is shown in the displacement vs. length (D-L) diagram (Fig. 5.7) where all

segments are linked and only accruing a displacement. At 48.2 % extension and 32 seconds have F2 reached 180 mm in length and 5,5 mm in maximum heave.

Fault segment behaviours in D-L space

Plotting the above described segments as well as all smaller segments in the experiments in D-L space (Fig. 5.6 and 5.7) shows that almost all of the segments in this experiment exhibit elements of staged growth , exhibiting (i) lengthening with minimal displacement accumulation, before (ii) entering a stage of displacement accrual and limited lengthening, which in turn is followed by (iii) renewed lengthening and low-rate displacement accumulation in concert. Another stage (iv) is seen upon linkage and assembly of F1, which is arrested (by the walls) when it reaches 400 mm in length. After this, displacement accrual continues to the end of the experiment

The first diagram (Fig. 5.6) shows that segments start accruing a displacement between 9- and 38-mm. Segment S3 has the smallest length before accruing a displacement with the length ~9 mm, and segment S1 is the longest before accruing a displacement ~38 mm.
Segments S1 is the only measured segment that start to grow both in length and displacement from the start.
All segments are linked when the segment reached 400 mm and 12.65 mm in heave.

The second diagram (Fig. 5.7) shows segments growing proximity of F1. It shows the growth in a smaller scale, since these segments are smaller. The first segments measured start to accrue a displacement after lengthening 10 mm and the last segments lengthens 40 mm before accruing a displacement (Fig. 5.7).
A closer look at the details of these to diagrams shows that the segments grow in several periods in length and displacement.

Timestep Extension	Picture	Map

West   East

a)

T1
T=13 sec
E= 23,8 %

b)

c)

T2
T=16 sec
E=28 %

d)

e)

T3
T=21 sec
E=33,3 %

f)

g)

T4
T=24 sec
E=38,1 %

h)

i)

T5
T=32 sec
E= 48,2 %

j)
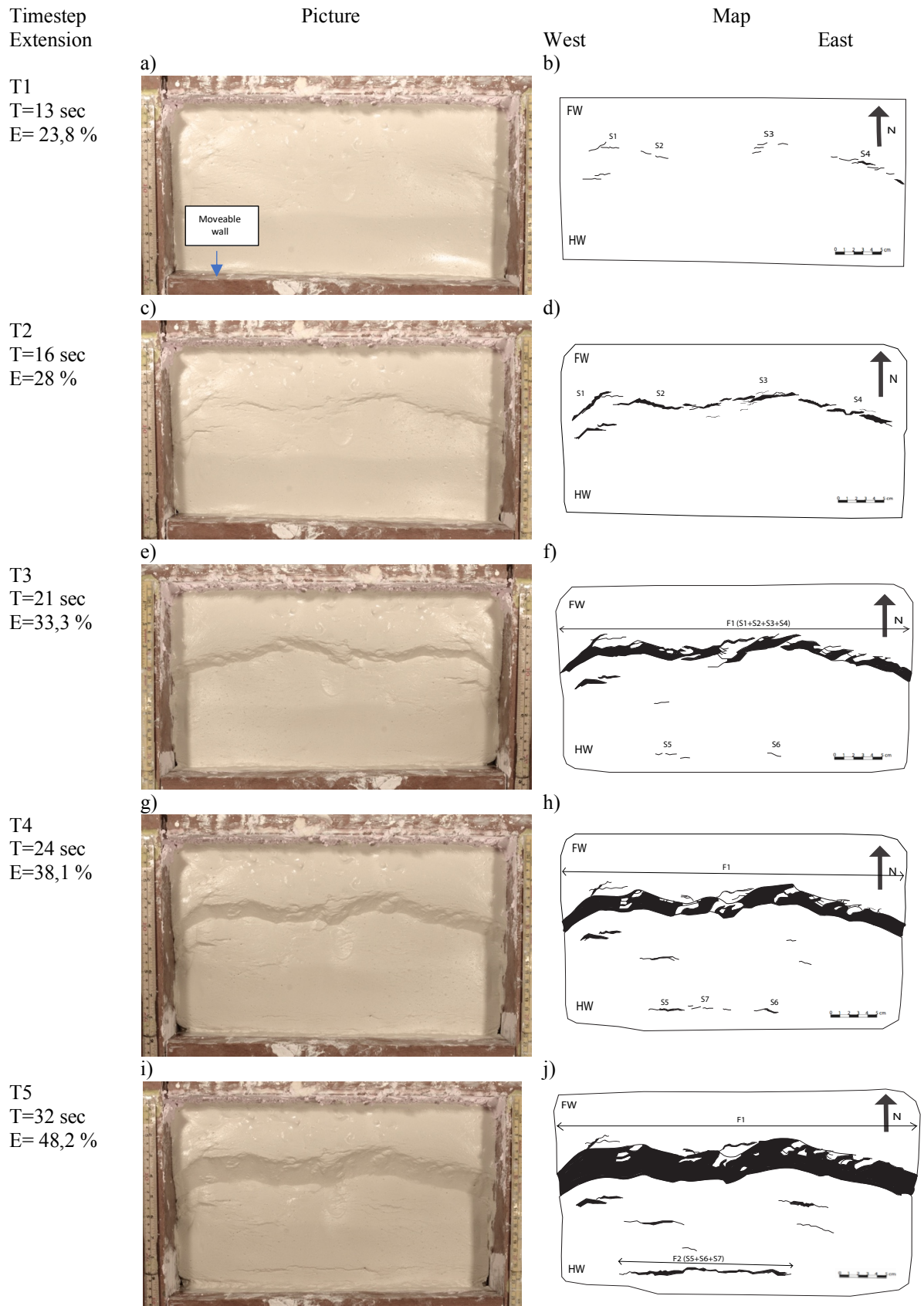
Figure 5.5: shows the evolution of an extensional regime in a plaster experiment. It is divided in to five timesteps (T1-T2) that accentuate the deformation that occur. The picture to the left shows the plaster model at given time and extension. To the right is an overview map of the deformation occurring in the picture beside. The moveable wall is to the south
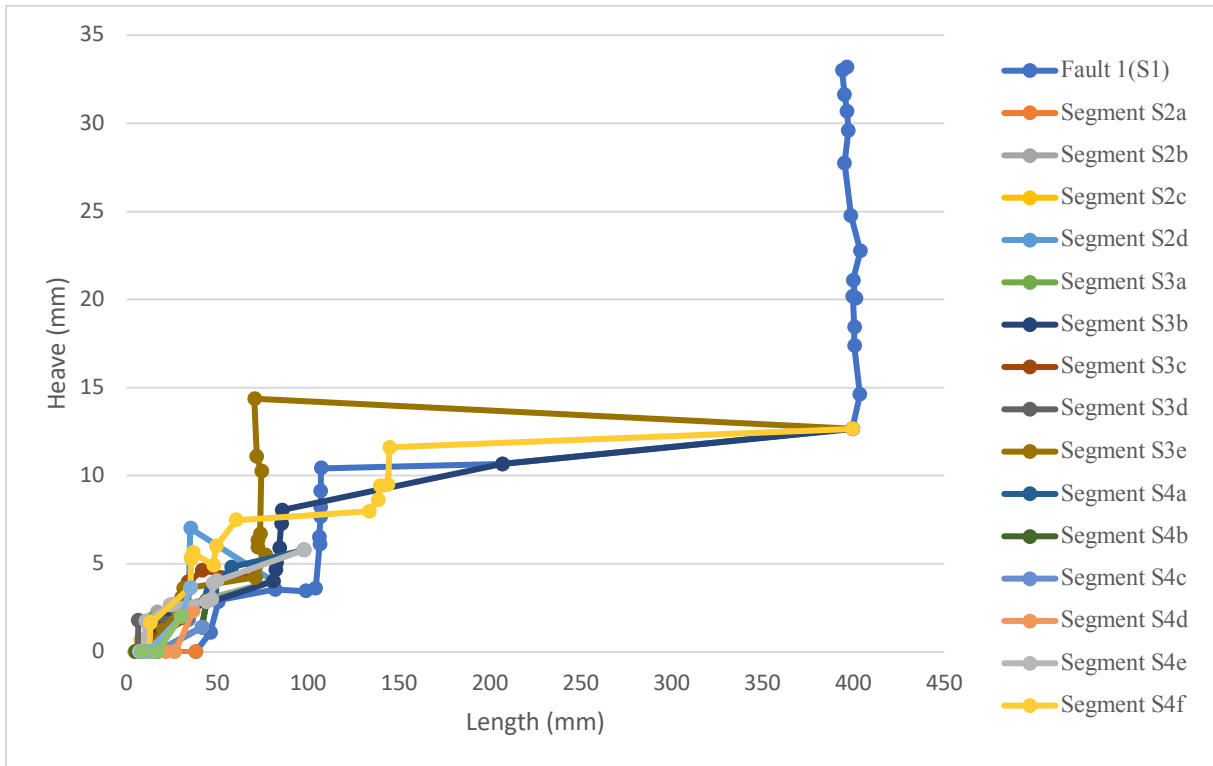
Figure 5.6: shows faults and fault segments related to the growth and assembly of fault F1. Note that upon arrest of the tips at the experiment boundary, the fault stops to lengthen and then accrues displacement (Fault F1).

Figure 5.7: shows all measured segments that occur outside the proximity of F1.

5.4 Description of experiment 3

Table 5: General information about experiment 3

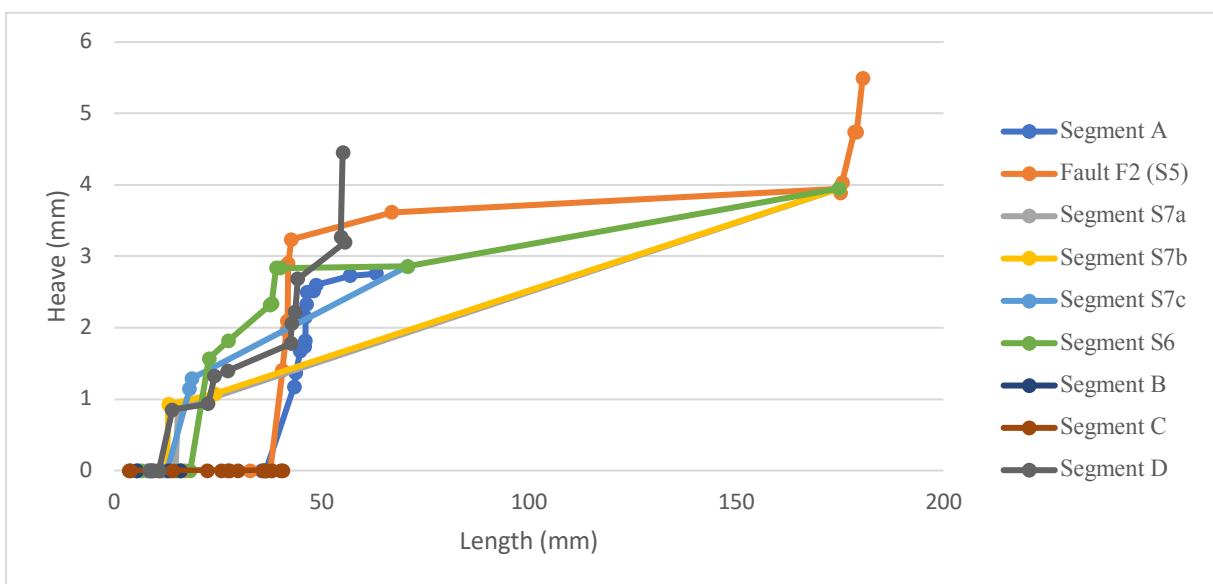|	
Date	25.11.2015
Plaster to water ratio	1:1.7
Basal layer	Wedge shape with () 15° slope
Initial length	173 mm
Final length	361 mm
Total displacement	188 mm
Total extension (%)	108.7
Duration	49 s
Mean extension rate	7.4 mm/s

General information of the evolving of the experiment

From zero to timestep T1 – 0-33 %:

After ~20.8 % extension and 9 seconds nucleates the first segments in the surface of the plaster. They grow mainly in an east-west direction perpendicular to the extensional (movable wall) direction (Fig. 5.8 a-b).

F1 grows along the northern wall and after 11 seconds and 25 % extension in to the experiment propagates its length from the wall in the east to the wall in the west.

Segment S1 and surrounded segments starts to grow at the same time (extension) as F1. They propagate rapidly in length and displacement. Some of the segments in this location dips in the opposite direction to the dip direction of the majority of the segments in the model (Fig. 5.8 a-b, marked with blue colour).

After 25 % extension and 10 seconds breaches sub-segments of segments S3 through the surface in the middle part of the model with the same east-west direction at the same time as F1. The sub-segments propagate as isolated segments and grows parallel and overlapping each other (Fig. 5.8 a-b).

After ~31 % extension and 13 seconds start segment S3 to accruing a displacement.

At the same time (extension) starts a single segment to grow in the west part of the model (S2), (Fig. 5.8 a-b). The segment grows by segments tip propagation.

<u>T1 to T2 – 33-68.2 %:</u>

After 35 % extension and 15 seconds breaches sub-segments of S4 through the surface near the east wall. They appear in parallel overlapping segments and start to grow in length with an east-west direction. The displacement is close to zero at this timestep.

Segment S1 and surrounding segments curves in length direction. The orientation on the segment-tip to the east have a north-east direction and the orientation on the segment-tip to the west has a north-west direction (as a smile in map view, Fig. 5.8). Also, created by an antithetic segment (marked blue in Fig. 5.8). One of the sub-segments of S1 propagate rapidly and have the largest maximum displacement, without taking F1 into account at T2.

Segment S2 and S3 is small single segments with a displacement close to zero. Nearly all the segmented faults (S2, S3 and S4) occurs in a line through the model.

Segment S3 splays from its original segment and in to a new path at ~38 % extension. The segment-tip propagate westward and after ~ 42 % extension linking with the overlapping segment to the south.

Relay ramp between segment S2 and S3 breaches in the lower part of the ramp by the segment-tip of S3. Segment S2 and S3 link together after 64.1 % extension. (This point where these segments links show very distinctly in the diagram (Fig. 5.9). Best shown where Fault 3a (yellow curve) meets Fault 2a (orange)).

Segments start to grow in the same place as segment S2 (to the north of the segment linking to F2) in the hanging wall F1 after ~ 48 % extension (Segment S2 a-c, Fig. 5.10).

F1 is the largest fault both in length and displacement.

<u>T2 to T3 – 68.2-84.4 %:</u>

The segment in the hanging wall of the main fault F1 (to the north of segment S2) (Segment S2 a-c, Fig. 5.9), reaches its full length and displacement after 72.8 % extension. At 75 % extension and 29 seconds stops segment F1 accruing a displacement at 60 mm.

Segments in the same located as segment S1 have grown and overlapping each other, creating structures of horst and graben. When the main fault F1 stops accruing a displacement, stagnating the segments surrounding S1 and then stops growing in length and displacement.

45

New sub-segments of S5 breaches through the surface in the hanging wall of S2 and S3 when the main fault F1 stops growing. They start to propagate from the east in the center of the hanging wall towards southwest. The sub-segments of S5 propagate in an east-west direction and overlap each other in a transverse north-east south-west direction.

The segment-tip to S3 propagate rapidly, ~ 30mm in 1 second, towards segment S4.

At ~77.5 % extension overlap segment S3 and S4 each other creating a relay ramp. The ramp features small fractures crossing it.

The relay ramp breaches in the middle of the ramp after ~ 82 % and 32 seconds and fully link segment S2-S4 from the wall in the west to the wall in the east creating a main fault (F2).

T3 to T4 – 84.4-94.2 %:

F2 stops accruing a displacement after 93 % extension and have a maximum heave at 36 mm, measured to the west right above F2 in Fig 5.8f.

F2 start growing a new segment-tip where S3 (Fig. 5.8 e-f) was located abutting in to its hanging wall 2 second after F2 is fully liked. The tip propagates in 2 seconds before it stops lengthening with a south-west orientation and 60 mm in length.

The segments in the hanging wall of F1 are divided by (three) relay ramps.

The relay ramp, in the north-east, breaches first after 90 % extension by the segment-tip propagating northwards.

The seconds two relay ramps breaches after 92 % extension.

The relay ramp in the middle part of F1 breaches by small fracture breaching the middle part of the ramp.

The ramp, in the west, breaches by segment-tip propagating through the ramp, linking all the transverse sub-segments of S5 to each other (Fig. 5.8 g-h).

T4 to T5 – 94.2-100 %:

Segment S5 grows throughout the experiment and ends with ~257 mm in length direction and ~11 mm in maximum heave, measured in the middle of the segment (Fig. 5.8 j)

Fault segment behaviours in D-L space

Plotting the above described segments as well as all smaller segments in the experiments in D-L space (Fig. 5.9 and 5.10) shows that almost all of the segments in this experiment exhibit elements of staged growth, exhibiting (i) lengthening with minimal displacement accumulation, before (ii) entering a stage of displacement accrual and limited lengthening, which in turn is followed by (iii) renewed lengthening and low-rate displacement accumulation in concert. Another stage (iv) is seen upon linkage and assembly of F2, which is arrested (by the walls) when it reaches 400 mm in length. After this, displacement accrual continues to 75 % extension.

The first diagram (Fig. 5.9) shows that segments start accruing a displacement between 15,9- and 77,5 -mm. Segment S4b has the smallest length before accruing a displacement with the length ~15,9 mm, and segment S2 is the longest before accruing a displacement ~77,5 mm. Segments S4a is the only measured segment that start to grow both in length and displacement from the start. All segments are linked when the segment reached 400 mm developing a main fault (F1) with a maximum heave at 31mm. F1 accruing a displacement to 60 mm before it stops growing.

The second diagram (Fig. 5.10) shows segments growing proximity of F1. It shows the growth in a smaller scale, since these segments are smaller. The first segments measured start to accrue a displacement after lengthening 16,7 mm and the last segments lengthens 56,6 mm before accruing a displacement (Fig. 5.10).
A closer look at the details of these to diagrams shows that the segments grow in several periods in length and displacement.

Timestep Extension	Picture	Map

Map: West — East

T1
T= 14 sec
E= 33 %

T2
T=27sec
E= 68,2 %

T3
T= 33 sec
E= 84,4 %

T4
T= 36 sec
E= 94,2 %

T5
T= 40 sec
E= 100 %
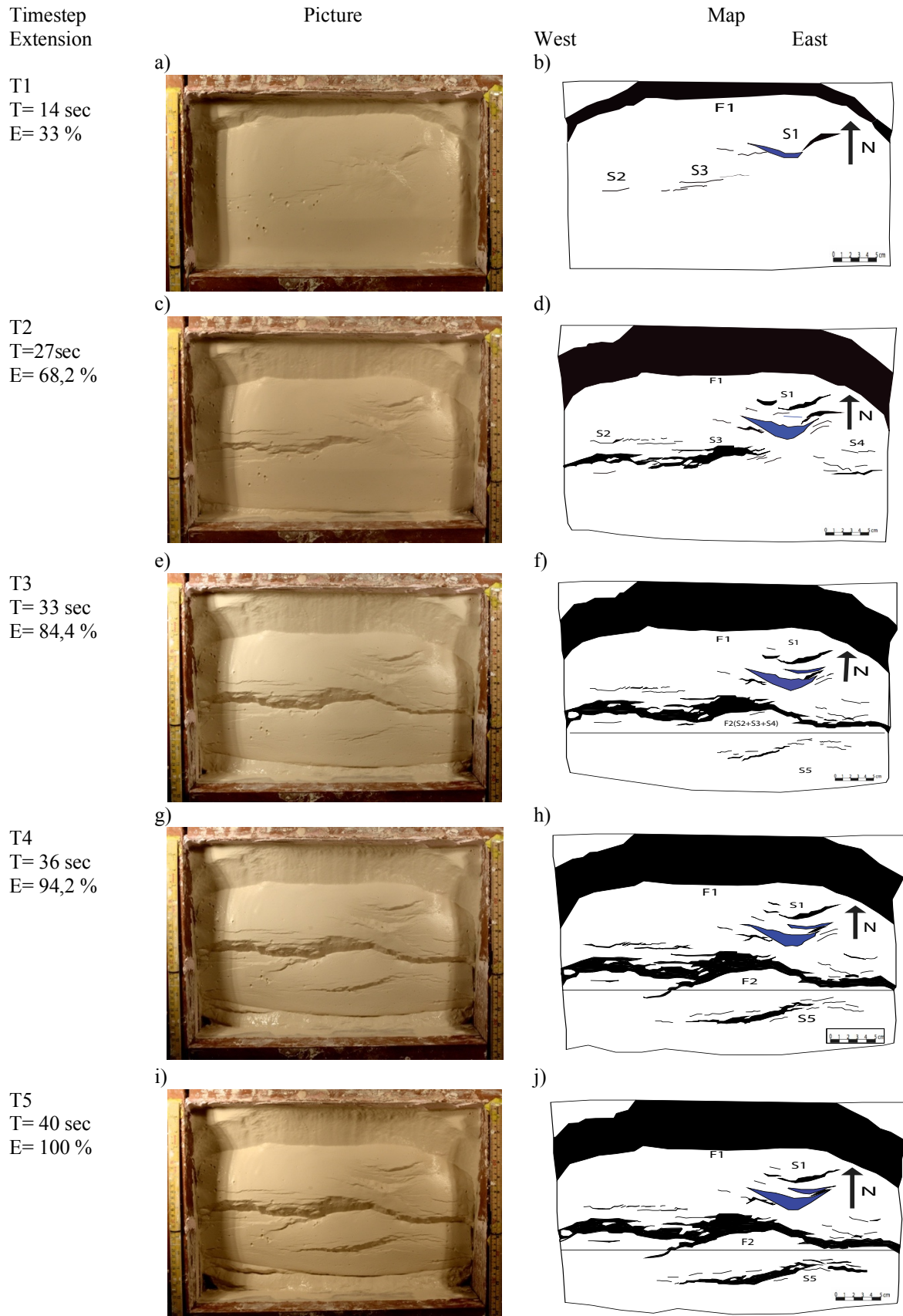
Figure 5.8: shows the evolution of an extensional regime in a plaster experiment. It is divided in to five timesteps (T1-T2) that accentuate the deformation that occur. The picture to the left shows the plaster model at given time and extension. To the right is an overview map of the deformation occurring in the picture beside. The moveable wall is to the south. Faults marked with blue colour dips in the opposite direction then the majority of the fault in the model

Figure 5.9: shows faults and fault segments related to the growth and assembly of fault F2. Note that upon arrest of the tips at the experiment boundary, the fault stops to lengthen and then accrues displacement (Fault F2).
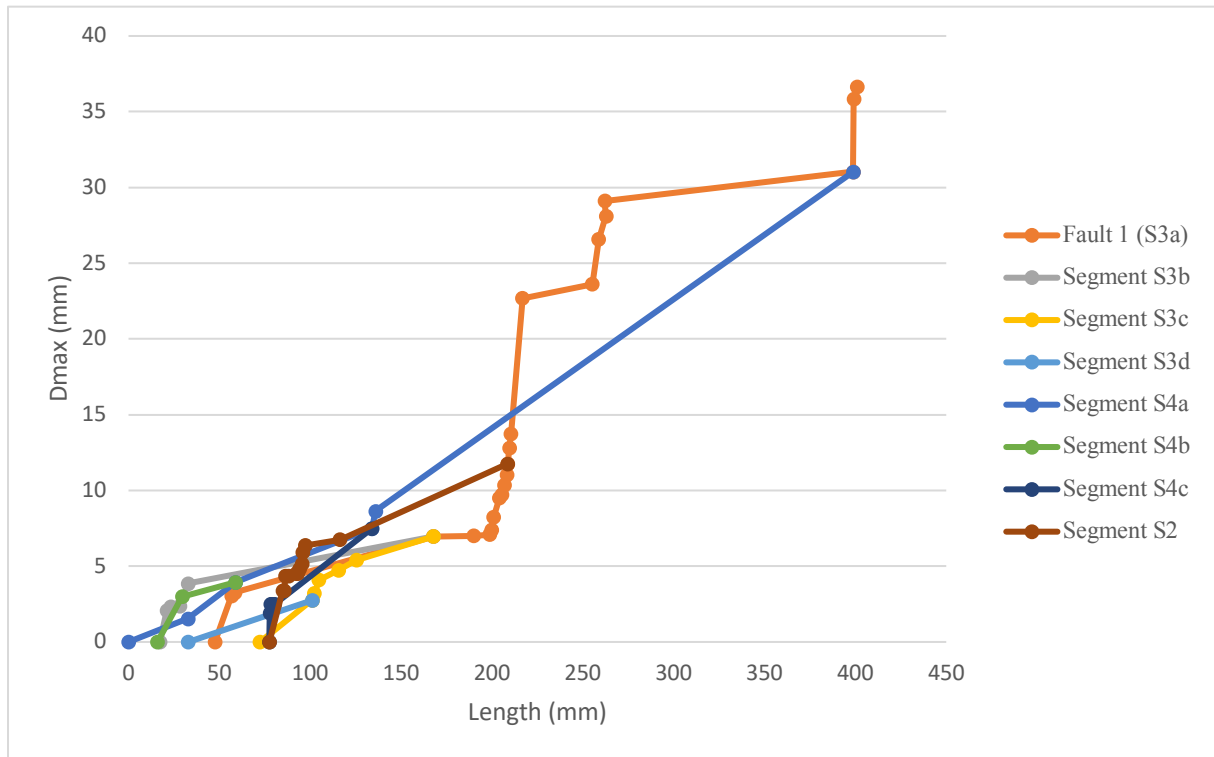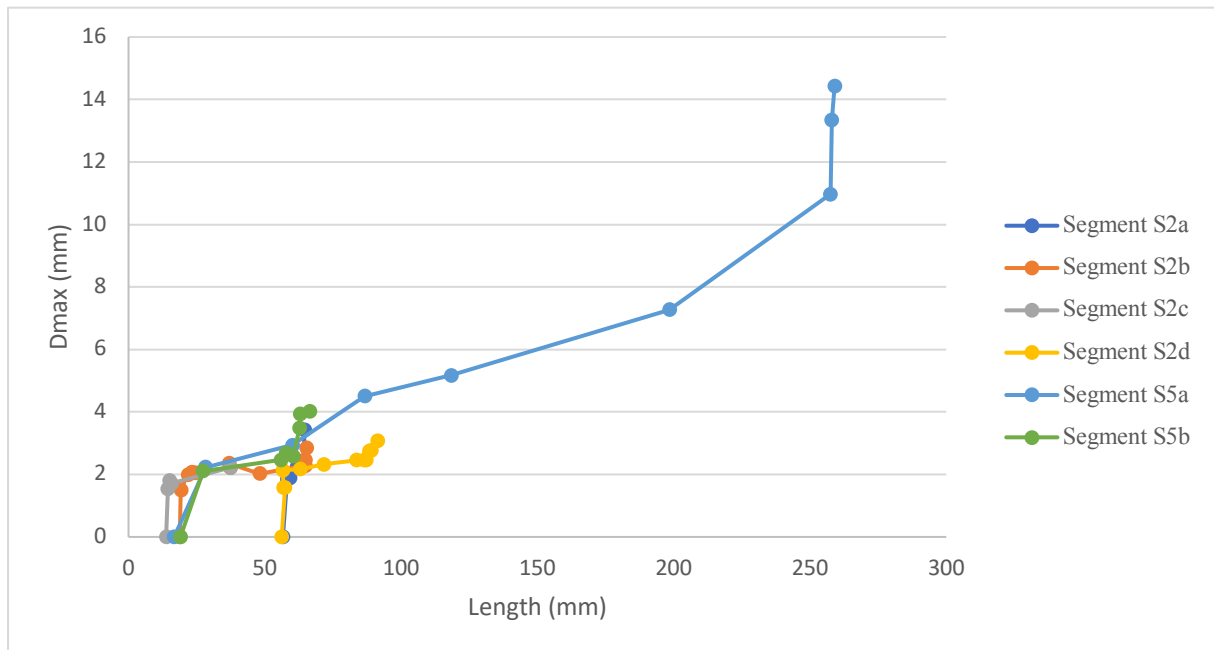

Figure 5.10: shows all measured segments that occur outside the proximity of F1.

5.5 Description of experiment 4

Table 5.4: General information about experiment 4

Date	10.12.2015
Plaster to water ratio	1: 1.7
Basal layer	Wedge shape with a () 15° slope
Initial length (mm)	148
Final length (mm)	296
Total displacement (mm)	148
Total extension (%)	100
Duration (second)	73
Mean extension rate (mm/s)	4

General information of the evolving of the experiment

From start to timestep T1 – 0-60.3 %

At ~ 43 % extension breaches the first visible fault segments through the surface. They are located in the middle part of the model as S1 and S2 (Fig. 5.11 a-b), both with an east-west orientation.

Segment S1 lengthens rapidly and dips in the opposite direction to the dip direction of the majority of the segments in the model (Fig. 5.11 a-b).

Segment S2 start to grow from the east wall and lengthens rapidly. It has reached its full length by timestep T1.

At 50 % extension are segments starting to grow along the wall in the north (Fig. 5.11 a-b). They are accruing a displacement rapidly.

The segment growing in the middle is formed as an V. It overlaps the segment to the west, that overlapping the segments between itself and the wall to the west.

Several new small segments start to grow especial localized around segment S1 (Fig. 5.11 a-b). They grow in an east-west direction overlapping each other (Fig. 5.11 a-b).

T1 to T2 – 60.3-85.6 %

After ~ 67 % extension are all the segments along the north wall fully linked from the wall in the east to the wall in the west (F1) (Fig. 5.11 c-d).

At T1 has segment S1, an antithetic segment, propagates both in the west and east tip and accruing a displacement. Small segments surrounding segment S1 accruing a dip in the same direction as the majority (Fig. 5.11 c-d).

Segment S2 are still accruing a displacement at this timestep.

New smaller sub-segments of S3 and S4 breaches through the surface to the south parallel to the moveable wall with an east-west orientation.

Segment S3 is the first of them to breach through the surface after ~ 80 % extension. In one second has it lengthens twice its own "start" length.

Segment S4 breaches through the surface as several small sub-segments (S4a and S4b) to the south in the mid part of the experiment (Fig 5.11 c-d) after ~82 % extension.

At ~ 84 % extension stops the main fault F1 to accruing a displacement at its west side, but still accruing a displacement in the east part of the fault.

At the same extension stop segment S1 accruing a displacement.

T2 to T3 – 85.6-89 %:

Small sub-segments breaches through the surface after ~ 86 % extension in the south part of the model where segment S5 is located.

Sub-segments of S4 overlapping each other (Fig 5.11 e-f). One of the small segments (S4a) propagates northwards towards a segment (S4b) to the north, creating a smile shown in the figure (Fig. 5.11 e-f).

At ~ 87 % extension stops the main fault F1 accruing a displacement at its east side. At the same time/percent extension stops segment S2 to accruing a displacement.

When main fault F1 has reached its maximum displacement breaches several new segments through the surface. Especially located to the south parallel to the moveable wall where segment S3, S4 and S5 is located.

T3 to T4 – 89-90.4 %:

After ~ 90 % extension links segment S4a and S4b together. Segment S4a tip continues to propagate northwards towards segment S4b and links together in the middle of segments S4b, creating an abutting pattern.

At the same extension are two sub-segments of S5 (S5a and S5b) propagating towards each other. They link together by their segment-tips (Fig. 5.11 g-h).

T4 to T5 – 90.4-100 %:

At ~ 91 % extension are all the sub-segments of S3 linked. This occurs when the segment to the west starts to curve and propagate northwards, breaching in the middle of the relay ramp dividing them.

The relay ramp dividing segments S3 and S4 breaches at the same extension. This occurs by segment S3 tip curving and propagate northward towards segment S4. Segment S3 links in the middle of segment S4 and arrest the tip on its west side (Fig 5.11 i-j).

At ~ 93 % extension breaches the ramp in between segment S4 and S5. Small already existing fracture accruing a displacement in the middle of the ramp and linking the two segments together.

The last relay ramp, southeast in the model where segment S5 is located, breaches in the lower part of the ramp. The segment to the east propagates westward and links together with segment S5. Arresting segment S5 tip to the east. This links all the segment S3, S4 and S5 together. Creating a fully linked main fault (F2) from the wall to the east to the wall in the west (Fig. 5.11 i-j). This event occurs at the end of the extension. Fault F2 heave is 15.8 mm and is measured in the middle of where S3 and S4 would be in F2.

Fault segment behaviours in D-L space

Plotting the above described segments as well as all smaller segments in the experiments in D-L space (Fig. 5.12 and 5.13) shows that almost all of the segments in this experiment exhibit elements of staged growth , exhibiting (i) lengthening with minimal displacement accumulation, before (ii) entering a stage of displacement accrual and limited lengthening, which in turn is followed by (iii) renewed lengthening and low-rate displacement accumulation in concert. Another stage (iv) is seen upon linkage and assembly of F2, which is

arrested (by the walls) when it reaches 400 mm in length. After this, displacement accrual continues to in reaches 93 % extension of the experiment.

The first diagram (Fig. 5.12) shows that segments start accruing a displacement between 24- and 47.5 -mm. Segment S4a has the smallest length before accruing a displacement with the length 24 mm, and segment S5a is the longest before accruing a displacement 47.5 mm. All segments are linked when the segment reached 400 mm in length and 15.8 mm in heave.

The second diagram (Fig. 5.13) shows segments growing proximity of F1. The first segments measured start to accrue a displacement after lengthening 5.8 mm and the last segments lengthens 85.1 mm before accruing a displacement (Fig. 5.13).

Timestep Extension	Picture	Map
		West East

a)

T1
T=41 sec
E=60,3 %

b)

c)

T2
T=52 sec
E=85,6 %

d)

e)

T3
T=57 sec
E=89 %

f)

g)

T4
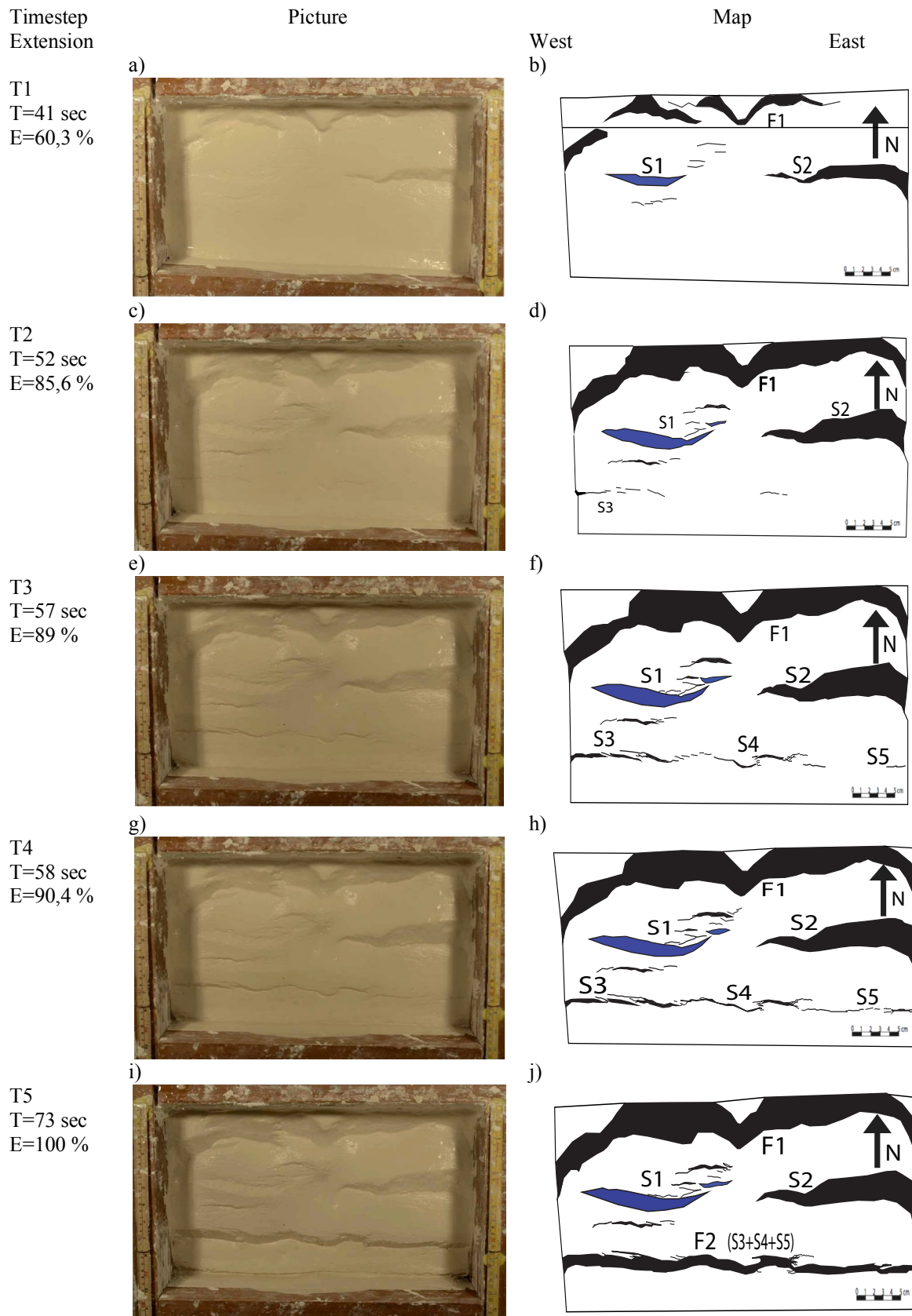T=58 sec
E=90,4 %

h)

i)

T5
T=73 sec
E=100 %

j)

Figure 5.11: shows the evolution of an extensional regime in a plaster experiment. It is divided in to five timesteps (T1-T2) that accentuate the deformation that occur. The picture to the left shows the plaster model at given time and extension. To the right is an overview map of the deformation occurring in the picture beside. The moveable wall is to the south. Faults marked with blue colour dips in the opposite direction then the majority of the fault in the model
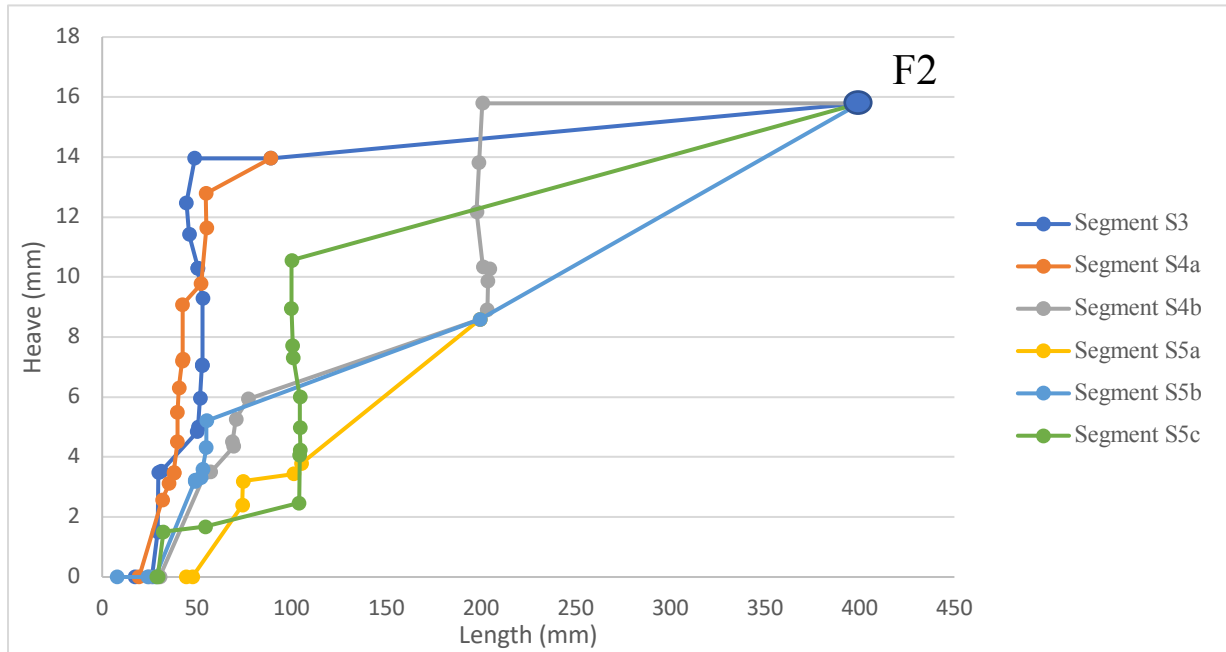
Figure 5.12: shows faults and fault segments related to the growth and assembly of fault F2. Note that upon arrest of the tips at the experiment boundary, the fault stops to lengthen and then accrues displacement (Fault F2).
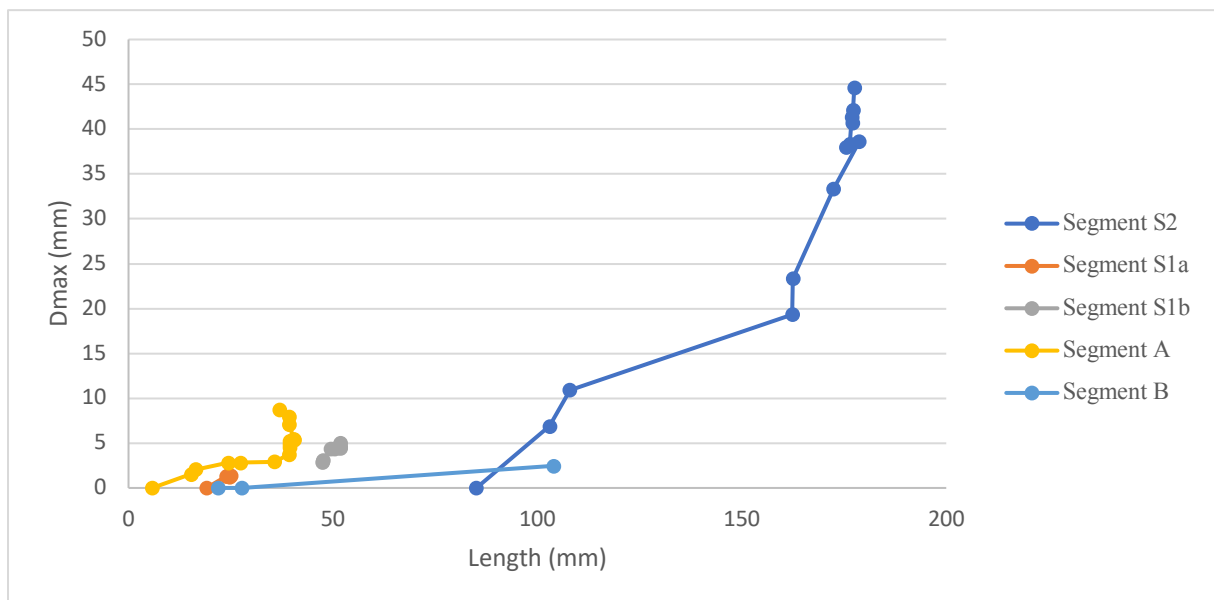

Figure 5.13: shows all measured segments that occur outside the proximity of F2.

CHAPTER 6 – DISCUSSION

6.1 Introduction

Four analogue plaster models have been analysed for this master project. They have been studied and quantified to investigate the relationship between lengthening and displacement for several fault segments in the extensional regime and a detailed description of how the faults grow have been presented. The results are discussed and interpreted in this chapter and it will be focusing on the main objectives for this thesis.

6.2 Basal layer geometry

The experimental setup used for this project is a simple analogue model of an extensional regime.

Experiments 1 and 2 have a horizontal arranged barite layer and experiments 3 and 4 have a wedge shape barite layer. Both experiment 1 and 2 have one main fault (F1) located in the middle of the model with an east-west direction when the experiments end (Fig. 5.2 and 5.7). When the displacement of the main fault (F1) stagnates or stop accruing, occurs an increase in the growth of smaller fault segments mainly in the hanging wall of F1.

Experiments 3 and 4 have two main faults (F1 and F2) breaching through the models at the end of the experiments (Fig. 5.8 and 5.11). The first main fault (F1) that breaches through the surface is located along the north wall for both of the models. When the displacement of F1 stagnates and/or stops accruing, occur an increase in the growth of the fault segments in the hanging wall, developing a second fully linked main fault (F2). This information indicates that the shapes of the barite basement influence the evolution of faults and how they are distributed in the surface. According to Fossen and Rotevatn (2016), the rheology and/or heterogeneity of the underlying crust may influence faulting, for example where a basal mobile salt layer affects the fault distribution and growth in the overburden, or where a pre-existing network of faults controls the localisation and orientation of new generations of faults. The wedge-shaped barite has a great influence from the shear-stress due to the incline of its layer, while the horizontal layer has a greater affect from the normal stress. This affects the result of the fault growth in the experiments. The fault distribution is also restricted by the experiment boundary and the properties in the rheology of the plaster.

The rheology of the plaster is similar for experiment 1, 2 and 3 when the experiment starts, while the rheology of the plaster to experiment 4 are more ductile than the others. This appears clearly in the interpretation of the experiments. The first fault segments that starts to grow in experiment 4, shows signs that the plaster is still (very) ductile when the experiment starts. This is specially highlighted for the evolution of F1. The plaster exhibits no ´hard lines´ in the model to interpret. The structures have soft and curved shapes and leaves evidence to suggest that the faults have grown from plaster 'sinking' but still develops a fault segment structure. This is very likely since its only used a screw to control the plasters consistent and determine when the experiment is ready to start (ch. 4).

There are distinct differences between the two main faults, F1 and F2, in experiments 3 and 4. F1 is established from one or linked by few large fault segments, while F2 is linked by several small fault segments. The properties of the rheology of the plaster has changed from the start of the experiment to the end. The faults evolving early in the experiment shows properties of a ductile rheology (F1), while the faults evolving at a later time shows signs that they have grown and linked in a brittle rheology (F2). The second main fault (F2) for experiments 3 and 4 are more similar to the main fault (F1) in how they grow and their geometry in the surface.

6.3 Normal fault growth

6.3.1 Description of normal fault growth from the models

The first fault segments nucleate through the surface between 17-43 % extension of the models. Experiments 1, 2 and 3 have a smaller difference between the nucleation of fault segments. The percentage extension for the first fault segments is only between 17-23,2 % for these experiments. The rheology of the plaster is more ductile for experiment 4, explained in the section above. In experiment 4 nucleates the first fault segment the surface after 43 % extension. The majority of the faults lengthens in an east-west orientation, perpendicular to the extension direction in all of the experiment in regards to the stress principle described by Anderson (1905). In both of the experiments 1 and 2 nucleates the first fault in the middle of the experiments and in the experiments 3 and 4 nucleates the first fault segment along the north wall. The first faults propagating in the models overlap and link together, developing the main fault (F1 and F2). The period after they are linked consist of a displacement accruing

phase. When the main fault stops accruing a displacement increases the fault growth in its hanging wall. These fault segments grow asymmetrical to each other, creating an echelon formation of fault segments (Fig. 6.3).

6.3.2 Displacement – length relationship

Two displacement – length diagrams are plotted for each of the experiments. The first diagram shows trajectories for fault segments creating the main fault (F1 or F2). The second diagram shows trajectories for fault segments growing outside the proximity of the main fault or faults.

6.3.3 Displacement-length diagram compared to fault growth models

By analysing the displacement-length diagrams in detail, is it clear that the fault segments grow different in relations with each other based on the length and displacement ratio. Four stages can be recognized based on the displacement-length diagrams. The first stage (i) exhibit the growth in the beginning when the fault propagating in length direction with minimal displacement accumulation. Then the faults enter the second stage (ii) where it consists of displacements accrual and limited lengthening. Some of the smaller fault segments measured in the experimental models stops growing in this stage. These two stages is comparable to the description of the constant-length fault growth model (Jackson et al., 2017; Rotevatn et al., 2018; J. Walsh et al., 2003; J. Walsh et al., 2002), which says that faults reaches its near final length early in the slip history before entering a phase with displacement accruing.

Then enters the fault segments a third stage (iii) with renewed lengthening and low-rate displacement accruing. The last recognized stage (iv) consist of fault segments linkage and a fully linked fault. The fault can only grow by displacement accrual. The (iii) stage shows that the fault grows in a more synchronously trajectory than for the first stage (i) that mostly grow by lengthening. The last two stages (iii) and (iv) illustrate a renewed sub-vertical version of the constant-length fault growth model. Rotevatn et al. (2018) concludes that the normal fault growth is characterized by hybrid growth behaviour. By studying these trajectories in detail, it is clear that the faults grow more complex than the two models manage to provide of information in this environment, however they give a good foundation to illustrate the larger trends for fault growth. An overall description of the occurrence in the diagram can be staged

in two periods. The first period consists of a synchronously growth between the displacement and length relationship and is similar to the propagating fault model. The second stage which consist of displacement accruing can be compared to the constant-length fault growth model. This information extracted from the displacement-length ratio diagrams gives a greater confirmation to the conclusion suggested by Rotevatn et al. (2018).

6.3.4 Displacement-length diagram compared with the evolution in the experimental models

The four periods identified by tracing the trajectories of fault growth in the displacement – length diagrams can be compared to the four stages proposed for relay ramps by Peacock and Sanderson (1991). The first phase (i) exhibiting lengthening with minimal displacement accumulation. In the model is this recognized as the period when small isolated fault segments nucleate and breach the surface. The smallest nucleated fault length is measured to be 1,5 mm. This measurement illustrates how small the fault segments interpreted are for this project. The majority of the fault segments Majority of the fault segments stagnant or stop propagating in length direction between 5-50 mm. This period (i) can be compared to the first stage introduced by Peacock and Sanderson (1994) regarding the evolution of relay ramp and represents the growth of isolated fault with no overlapping or interaction with other fault segments. The second phase (ii) starts when the fault segments enters a stage of displacement accrual and limited lengthening. In the model is this compared to the period with overlapping and soft-linked fault segments (Fig. 6.1a) and when they propagate in nearby fault segments stress drop zone. This can be compared to stage two introduced by Peacock and Sanderson (1991) and represent the first interaction through ductile strain. The third phase identified (iii) is a renewed lengthening and low-rate displacement accumulation in concert. This is recognized in the model as the period when faults lengthening efficient by linking with adjacent fault segments. Peacock and Sanderson (1991) did also characterise this by fracturing across the relay ramp (Fig. 6.2a) resulting in linkage between the two fault segments. Several factors as strain, the availability of faults and their distribution and arrangements etc. controls the linkage and breaching of a relay ramp (Fossen & Rotevatn, 2016). However, for this type of experiment is it the rheology of the plaster, shape of the basal layer, the extension distance and not at least the ratio of the extension of great importance as well. The last phase (iv) describes a fully linked fault with the fault tips in arrest. In the experimental models is this when the main faults (F1 and F2) is fully linked and arrested by

the walls with a length of 400 mm. These walls may not be natural to find in this kind of setting and geological events, but may illustrate other factors controlling the ability for a fault to lengthening. An example could be change in lithology for a sedimentary rock (Wilkins & Gross, 2002) or by the walls illustrating an already existing fault and that the main fault link together in the middle part of the existing fault, creating an abutting pattern (Fig. 2.8) (Nixon et al., 2014). The last stage in the evolution of a relay ramp by Peacock and Sanderson (1991) represents the breaching of the relay ramp. Although the four stages characterised by Peacock and Sanderson (1991) illustrate one structure were the for stages for the evolution of a relay ramp also useful to illustrate the four stages exhibit from the displacement – length diagram.

6.3.5 Breached relay ramp

Three types of relay ramp breach are observed in the experimental models. The majority of the relay ramps breaches in the lower part of the ramp in the hanging wall. This occur often by the fault tip to the segments to the south start curve towards the overlapping fault segment to the north, forming a ramp breach in the lower part of the ramp (similar to the single breach illustrated in fig. 2.5b and can also be recognized in figure 6.2 and 6.3). Mid-ramp breach is observed when the experiment has extended for some time (6.1 and 6.2). The relay ramp often contains fractures propagating in the ramp before a mid-ramp breaches and is shown in figure 6.2. Fractures can be located in the upper-, middle- and the lower part of the relay ramp and can be of interest to illustrate future breach in the ramp, however it was no clear assumption for this in these experimental models.

A few double breached relay ramps are observed in the experimental models as well. These have had the same starting point as the majority of the breached relay ramp (single-tip breach). If the two linked fault segments are allowed to continue to grow and accruing further displacement, starts the arrested fault tip of the segment to the north to propagate curving and link with the fault segments to the south a second time. This may or may not indicate that if the experiment had extended/lasted longer more faults would have the time to link a second time, creating double breached ramps. It can also be presumed that this only occurred for this situation and that the fault tips behave inactive after the single tip breach (Fossen & Rotevatn, 2016).

One of the factors that controls how the relay ramp breaches is the rheology of the plasters. The properties of the rheology changes throughout the experiment. In the beginning when the

experiment starts is the rheology more ductile, in this period breaches the ramp only by a single tip in the lower part of the experiment. The mid-ramp breach appears later when the rheology of the plaster is more brittle. It has been argued that the relay ramp needs a specific inclination to breach in the middle of the ramp, but this is not possible to investigate for these models since it is only the end result of the model that is preserved.
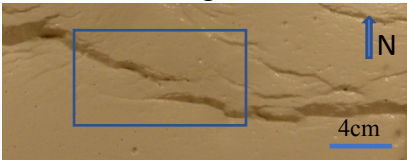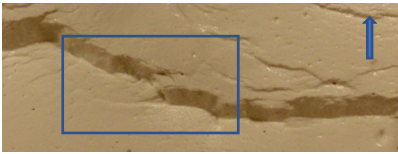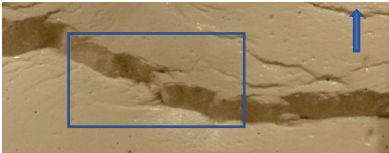
Mid-ramp breach	West East
T1 T = 0 sec Overlapping fault segments	a) Soft-linkage
T2 T = 2 sec Breached relay ramp	b) Hard-linkage
T3 T = 4 sec	c)

Figure 6.6: Shows how a relay ramp breaches with three timesteps (T1-T3) separated by 2 seconds. a) shows a relay ramp from experiment 3, b) shows how the ramp breaches in the middle, c) shows the further evolution for the breached ramp.
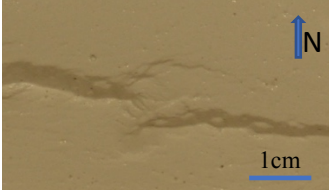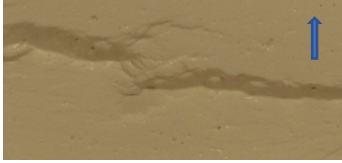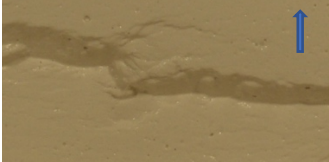
Fracture in the relay ramp		
	West	East
T1 T = 0 sec Fracture in the relay ramp		
T2 T = 3 sec Fractures crossing the relay ramp		
T3 T = 6 sec		

Figure 6.7: illustrate fracturing in the ramp and where the ramp breach with timesteps separated with 3 seconds. a) shows fracture in the ramp, b) shows how the fracture crosscutting the relay ramp and c) shows how the relay ramp breaches in the lower part of the ramp

En echelon faults	West East
T1 T = 0 sec Asymmetrical fault pattern	
T2 T = 1 sec Lower-ramp breach	
T3 T = 2 sec	

Figure 6.8: illustrate an echelon fault pattern separated with 1 second for each timestep. This is typical for fault segments occurring in the hanging wall of the main fault for several of the experiments. a) shows where the fault segments breach the surface and overlapping pattern, b) shows how the fault segments propagate towards each other and link, c) shows the evolution for this experiment. This fault can be recognized in the D-L plot (Fig. 5.10) as segment S5a.

6.4 Topology

It is important to study the fracture network because the topology can give new information to the fault network. Several fractures network can have the same geometrical factors as measurements, spatial orientation of the fault segment, trace length, area and volume, but without description of topology it easily could be misinterpreting the physical properties in the sub-surface (Sanderson & Nixon, 2015).

6.5 Nature

6.5.1 Global D-L dataset

The majority of the D-L trajectory from all of the experiments are plotted in to the log-log space from (Rotevatn et al., 2018). These D-L trajectories are marked with red colour (Fig. 6.4) and fall within the cloud in global D-L dataset in the same area as the analogue models that have been studied before. This log-log plot shows limited information about the different D-L trajectories of fault growth (Rotevatn et al., 2018), but it provides more evidence on the existing theory about the relationship between fault length and maximum displacement over many orders plotted in the global D-L dataset (Kim & Sanderson, 2005).
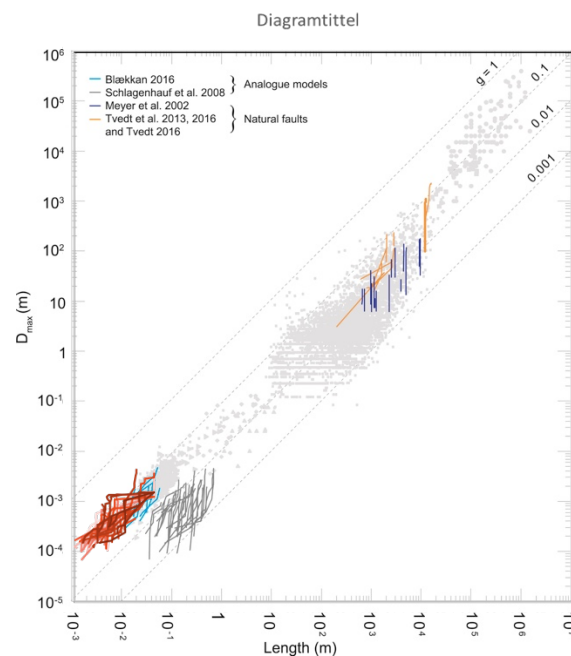

Figure 6.4: log-log space with plots from faults in nature and analogue models. Red lines demonstrate faults measured form this project. From (Rotevatn et al., 2018)

Comparing and combining relationship between different environment and techniques needs to be considered carefully and with understanding.

CHAPTER 7 – CONCLUSION

7.1 Conclusion

The main focus of this project has been to study the fault growth in several plaster experiments. These models have been performed as analogue experiments for an extensional regime. Measurements from the length and heave of subsegments, fault segments and main fault have been retrieved in timesteps and plotted in diagrams to be analysed and hopefully give some new information for further research. The main conclusions for this project are as follows:

- The evolution of structures in the model when the experimental models are completed is highly dependent on the properties of the rheology of the plaster during the experimental performance.
- In the environment presented in these analogue experiments the majority of the relay ramp breaches in the lower part of the ramp, in the surface of the hanging wall, between two fault segments.
- A few relay ramp breaches through the middle of the ramp. This occur in the context of the fact that small fractures have already been formed in the ramp, which eventually link the two overlapping faults together. This is observed in the later phase of the experiments.
- A double breached relay ramp is observed as well. This formed first as a single breached relay ramp (same as the majority), but with further extension there are few fault segments that breaches the ramp for a second time. This is not consistent.
- Displacement-length diagrams studied in detail shows that almost all of the fault segment in the experimental models grows with exhibit elements of staged growth:
  - (i)   lengthening with minimal displacement accruing
  - (ii)   displacement accruing and limited lengthening
  - (iii) renewed lengthening and low-rate displacement accumulation
  - (iv) Fully linked faults (arrested fault tips) and displacement accruing
- The two points described above confirms that the growth pattern for the fault segments in this environment grows as a hybrid between the 'propagating' and 'constant-length' fault growth models.

- The trend of the displacement-length relationship studied overall consist of two stages. The first is a synchronously fault growth between heave and length, and the second stage consist of displacement accrual

- The displacement-length trajectories fall within the Global data set and support the fault growth analysed in plaster models to be trust worthy to scale faults occurring in nature.

7.2 Proposal for further work

By investigate already existing experimental models or/and perform new analogue models based on extensional regime it is possible to extract new information that can provide a greater understanding of the complexity in fault growth. Some suggestions for future work are listed below:

- Perform multiple experiments with different shapes of basal layers and study how the different models evolve in the extension regime based on the substrate and compare them to natural events.

- Quantify more structures based on geometry and kinematics to make the structures easier to compare both in analogue models and in nature, for example relay ramps.

- Analyse the topology and geometry of the evolution of fracture network

- Investigate and characteristics the connectivity in a fault network

- Investigate the evolution of length and displacement with quantification in the model by taking time in to consideration.

- Use other types of experiments, different type of material or new types of equipment to perform an extensional regime so it is possible to compare the structures to already existing information.

REFERENCES

Ackermann, R. V., Schlische, R. W., & Withjack, M. O. J. J. o. S. G. (2001). The geometric and statistical evolution of normal fault systems: an experimental study of the effects of mechanical layer thickness on scaling laws. *23*(11), 1803-1819.

Anderson, E. M. (1905). The dynamics of faulting. *Transactions of the Edinburgh Geological Society, 8*(3), 387-402.

Barnett, J. A., Mortimer, J., Rippon, J. H., Walsh, J. J., & Watterson, J. J. A. B. (1987). Displacement geometry in the volume containing a single normal fault. *71*(8), 925-937.

Cadell, H. M. J. E., & Edinburgh, E. S. T. o. T. R. S. o. (1889). VII.—Experimental Researches in Mountain Building. *35*(1), 337-357.

Cartwright, J. A., Trudgill, B. D., & Mansfield, C. S. (1995). Fault growth by segment linkage: an explanation for scatter in maximum displacement and trace length data from the Canyonlands Grabens of SE Utah. *Journal of Structural Geology, 17*(9), 1319-1326.

Cloos, E. (1981). Experimental analysis of Gulf Coast fracture patterns.

Cloos, E. J. G. S. o. A. B. (1955). Experimental analysis of fracture patterns. *Geological Society of America Bulletin, 66*(3), 241-256.

Cowie, P. A., & Scholz, C. H. J. J. o. S. G. (1992a). Displacement-length scaling relationship for faults: data synthesis and discussion. *14*(10), 1149-1156.

Cowie, P. A., & Scholz, C. H. J. J. o. S. G. (1992b). Physical explanation for the displacement-length relationship of faults using a post-yield fracture mechanics model. *14*(10), 1133-1148.

Daubrée, A. (1879). *Etudes synthétiques de géologie expérimentale* (Vol. 2): Dunod.

Daubrée, G. A. (1878). *Expériences tendant à imiter des formes diverses de ploiements, contournements et ruptures que présente l'écorce terrestre*: Gauthier-Villars.

Dawers, N. H., & Anders, M. H. (1995). Displacement-length scaling and fault linkage. *Journal of Structural Geology, 17*(5), 607-614.

Favre, A. J. N. (1878). The formation of mountains. *19*, 103-106.

Fossen, H. (2016). *Structural geology*: Cambridge University Press.

Fossen, H., & Gabrielsen, R. H. (1996). Experimental modeling of extensional fault systems by use of plaster. *Journal of Structural Geology, 18*(5), 673-687.

Fossen, H., & Rotevatn, A. (2016). Fault linkage and relay structures in extensional settings—A review. *Earth-Science Reviews, 154*, 14-28.

Giba, M., Walsh, J., & Nicol, A. (2012). Segmentation and growth of an obliquely reactivated normal fault. *Journal of Structural Geology, 39*, 253-267.

Graveleau, F., Malavieille, J., & Dominguez, S. J. T. (2012). Experimental modelling of orogenic wedges: A review. *538*, 1-66.

Hall, J. (1815). II. On the Vertical Position and Convolutions of certain Strata, and their relation with Granite. *Earth and Environmental Science Transactions of the Royal Society of Edinburgh, 7*(1), 79-108.

Henza, A. A., Withjack, M. O., & Schlische, R. W. J. J. o. S. G. (2010). Normal-fault development during two phases of non-coaxial extension: An experimental study. *32*(11), 1656-1667.

Horsfield, W. J. F. T. i. N. E. (1977). An experimental approach to basement controlled faulting.

Horsfield, W. J. J. o. S. G. (1980). Contemporaneous movement along crossing conjugate normal faults. *2*(3), 305-310.

Hubbert, M. K. (1937). Theory of scale models as applied to the study of geologic structures. *Bulletin of the Geological Society of America, 48*(10), 1459-1520.

Hus, R., Acocella, V., Funiciello, R., & De Batist, M. J. J. o. S. G. (2005). Sandbox models of relay ramp structure and evolution. *27*(3), 459-473.

Jackson, C. A.-L., Bell, R. E., Rotevatn, A., & Tvedt, A. B. (2017). Techniques to determine the kinematics of synsedimentary normal faults and implications for fault growth models. *Geological Society, London, Special Publications, 439*, SP439. 422.

Kim, Y.-S., & Sanderson, D. J. J. E.-S. R. (2005). The relationship between displacement and length of faults: a review. *68*(3-4), 317-334.

Koyi, H. (1997). Analogue modelling: from a qualitative to a quantitative technique—a historical outline. *Journal of Petroleum Geology, 20*(2), 223-238.

Lindanger, R., Øygaren, M., Gabrielsen, R., Mjelde, R., Randen, T., & Tjøstheim, B. J. F. B. (2004). Analogue (plaster) modelling and synthetic seismic representation of hangingwall fault. *22*(1), 33-41.

Mandl, G. (1988). Mechanics of tectonic faulting. Models and basic concepts. Elsevier, Amsterdam, 407 p.

Mansfield, C., & Cartwright, J. (2001). Fault growth by linkage: observations and implications from analogue models. *Journal of Structural Geology, 23*(5), 745-763.

McClay, K., & Ellis, P. J. G. S., London, Special Publications. (1987). Analogue models of extensional fault geometries. *28*(1), 109-125.

McClay, K., & Scott, A. J. T. (1991). Experimental models of hangingwall deformation in ramp-flat listric extensional fault systems. *188*(1-2), 85-96.

Nixon, C. W., Sanderson, D. J., Dee, S. J., Bull, J. M., Humphreys, R. J., & Swanson, M. H. J. A. B. (2014). Fault interactions and reactivation within a normal-fault network at Milne Point, Alaska. *98*(10), 2081-2107.

Peacock, D., Nixon, C., Rotevatn, A., Sanderson, D., & Zuluaga, L. (2016). Glossary of fault and other fracture networks. *Journal of Structural Geology, 92*, 12-29.

Peacock, D., & Sanderson, D. J. A. b. (1994). Geometry and development of relay ramps in normal fault systems. *78*(2), 147-165.

Peacock, D., & Sanderson, D. J. J. o. S. G. (1991). Displacements, segment linkage and relay ramps in normal fault zones. *13*(6), 721-733.

Peacock, D., & Sanderson, D. J. J. o. S. G. (1996). Effects of propagation rate on displacement variations along faults. *18*(2-3), 311-320.

Rotevatn, A., Jackson, C. A.-L., Tvedt, A. B., Bell, R. E., & Blækkan, I. (2018). How do normal faults grow? *Journal of Structural Geology*.

Saint-Gobain. (2019). Molda 3 normal. Retrieved from https://www.saintgobainformula.com/product/molda-3-normal

Sales, J. K. J. (1987). Tectonic models. 785-794.

Sanderson, D. J., & Nixon, C. W. (2015). The use of topology in fracture network characterization. *Journal of Structural Geology, 72*, 55-66.

Walsh, J., Bailey, W., Childs, C., Nicol, A., & Bonson, C. (2003). Formation of segmented normal faults: a 3-D perspective. *Journal of Structural Geology, 25*(8), 1251-1262.

Walsh, J., Nicol, A., & Childs, C. (2002). An alternative model for the growth of faults. *Journal of Structural Geology, 24*(11), 1669-1675.

Walsh, J. J., & Watterson, J. (1988). Analysis of the relationship between displacements and dimensions of faults. *Journal of Structural Geology, 10*(3), 239-247.

Walsh, J. J., & Watterson, J. J. G. S., London, Special Publications. (1991). Geometric and kinematic coherence and scale effects in normal fault systems. *56*(1), 193-203.

Watterson, J. (1986). Fault dimensions, displacements and growth. *124*(1-2), 365-373.

Wilkins, S. J., & Gross, M. R. J. J. o. S. G. (2002). Normal fault growth in layered rocks at Split Mountain, Utah: influence of mechanical stratigraphy on dip linkage, fault restriction and fault scaling. *24*(9), 1413-1429.

Willis, B. (1894). *The mechanics of Appalachian structure* (Vol. 13): US Government Printing Office.